Geophysical Journal International

Geophys. J. Int. (2017) **209,** 1660–1676
Advance Access publication 2017 March 22
GJI Geodynamics and tectonics

doi: 10.1093/gji/ggx116

Secular variations in zonal harmonics of Earth's geopotential and their implications for mantle viscosity and Antarctic melting history due to the last deglaciation

Masao Nakada[1] and Jun'ichi Okuno[2]

[1]*Department of Earth and Planetary Sciences, Faculty of Science, Kyushu University, Fukuoka* 819-0395, *Japan. E-mail: mnakada@geo.kyushu-u.ac.jp*
[2]*National Institute of Polar Research, Tachikawa* 190–8518, *Japan*

Accepted 2017 March 18. Received 2017 March 15; in original form 2016 December 26

SUMMARY

Secular variations in zonal harmonics of Earth's geopotential based on the satellite laser ranging observations, $\dot{J}_n$, contain important information about the Earth's deformation due to the glacial isostatic adjustment (GIA) and recent melting of glaciers and the Greenland and Antarctic ice sheets. Here, we examine the GIA-induced $\dot{J}_n$, $\dot{J}_n^{\rm GIA}$ ($2 \leq n \leq 6$), derived from the available geopotential zonal secular rate and recent melting taken from the IPCC 2013 Report (AR5) to explore the possibility of additional information on the depth-dependent lower-mantle viscosity and GIA ice model inferred from the analyses of the $\dot{J}_2^{\rm GIA}$ and relative sea level changes. The sensitivities of the $\dot{J}_n^{\rm GIA}$ to lower-mantle viscosity and GIA ice model with a global averaged eustatic sea level (ESL) of $\sim$130 m indicate that the secular rates for $n = 3$ and 4 are mainly caused by the viscous response of the lower mantle to the melting of the Antarctic ice sheet regardless of GIA ice models adopted in this study. Also, the analyses of the $\dot{J}_n^{\rm GIA}$ based on the available geopotential zonal secular rates indicate that permissible lower-mantle viscosity structure satisfying even zonal secular rates of $n = 2$, 4 and 6 is obtained for the GIA ice model with an Antarctic ESL component of $\sim$20 or $\sim$30 m, but there is no viscosity solution satisfying $\dot{J}_3^{\rm GIA}$ and $\dot{J}_5^{\rm GIA}$ values. Moreover, the inference model for the lower-mantle viscosity and GIA ice model from each odd zonal secular rate is distinctly different from that satisfying GIA-induced even zonal secular rate. The discrepancy between the inference models for the even and odd zonal secular rates may partly be attributed to uncertainties of the geopotential zonal secular rates for $n > 2$ and particularly those for odd zonal secular rates due to weakness in the orbital geometry. If this problem is overcome at least for the secular rates of $n < 5$, then the analyses of the $\dot{J}_n^{\rm GIA}$ would make it possible to put more convincing constraints on the lower-mantle viscosity structure and GIA ice model, particularly for the controversial Antarctic melting history in GIA community.

Key words: Earth rotation variations; Time variable gravity; Rheology: mantle.

1 INTRODUCTION

Rate of change of degree-two ($n = 2$) zonal harmonic of the Earth's geopotential, $\dot{J}_2$, is dominantly attributed to the Earth's deformation associated with the glacial isostatic adjustment (GIA) due to the last glacial cycle and therefore provides important constraints on mantle viscosity (e.g. Nakiboglu & Lambeck 1980; Sabadini *et al*. 1982; Yuen *et al*. 1982; Yoder *et al*. 1983; Rubincam 1984; Wu & Peltier 1984; Vermeersen *et al*. 1997; Tosi *et al*. 2005; Peltier 2007; Mitrovica *et al*. 2015; Nakada *et al*. 2015). The geodetically derived geopotential zonal secular rate is, however, significantly affected by recent melting of glaciers and the Greenland and Antarctic ice sheets (e.g. Peltier 1988; Sabadini *et al*. 1988; Ivins *et al*. 1993; Mitrovica & Peltier 1993; Nakada & Okuno 2003; Tosi *et al*. 2005; Mitrovica *et al*. 2015; Nakada *et al*. 2015), and therefore it is required to independently estimate the recent melting contribution in inferring mantle viscosity. An independent estimate of the $\dot{J}_2$ due to recent melting is actually possible. Roy & Peltier (2011) and Cheng *et al*. (2013) indicated a gradual deceleration in the rate of the decrease in J_2 after $\sim$1990 by analysing the satellite laser ranging (SLR) observations for the period of 1976–2011, which suggests that the changes in the more recent time-series are attributed to the impacts of surface mass redistribution due to recent melting. That is, the contribution from recent melting and GIA processes may be separable if we incorporate modern recent melting history taken from the IPCC 2013 Report (Vaughan *et al*. 2013). In fact, Nakada *et al*. (2015) estimated GIA-induced $\dot{J}_2$ of –(6.0–6.5) $\times 10^{-11}$ yr^{-1} by considering the geodetically derived $\dot{J}_2$ (Roy & Peltier 2011;

Cheng *et al*. 2013) and recent melting by Vaughan *et al*. (2013), and inferred two permissible solutions for the lower-mantle viscosity, $\sim 10^{22}$ and (5–10) $\times$ 10^{22} Pa s, based on the simple three-layer viscosity model characterized by elastic lithospheric thickness, upper- and lower-mantle viscosities (see also Mitrovica *et al*. 2015). However, Nakada & Okuno (2016) indicated that analyses of the $\dot{J}_2$ based on the two-layer lower-mantle viscosity model with two layers in the lower mantle (see Section 2.1) only require a viscosity layer higher than (5–10) $\times$ 10^{21} Pa s for a depth above the core–mantle boundary (CMB). Lau *et al*. (2016) inferred a similar solution for the lower-mantle viscosity from inversion study of the J_2 datum.

More detailed radial viscosity structure is derived from GIA studies using $\dot{J}_2$ and relative sea level (RSL) changes with different radial sensitivities to viscosity structure of the mantle (Lau *et al*. 2016; Nakada & Okuno 2016). For example, Lau *et al*. (2016) estimated a mean upper-mantle viscosity of $\sim 3 \times 10^{20}$ Pa s, average viscosity of 10^{21} Pa s from 670 to $\sim$1500 km depth and 10^{22}–10^{23} Pa s in the deep mantle based on the $\dot{J}_2$, postglacial decay times in Canada and Scandinavia, the Fennoscandian relaxation spectrum and late-Holocene differential sea level highstands at sites in Australia. Nakada & Okuno (2016) also inferred a similar viscosity solution for the upper mantle and in the deep mantle from the $\dot{J}_2$, sea levels at the Last Glacial Maximum (LGM) for Barbados (Fairbanks 1989; Peltier & Fairbanks 2006) and Bonaparte Gulf in Australia (Yokoyama *et al*. 2000), and late-Holocene differential sea level highstand for Karumba and Halifax Bay in Australia (Nakada & Lambeck 1989). However, the lower-mantle viscosity above the mid-lower mantle is higher than that by Lau *et al.* (2016); namely, higher than 3×10^{21} Pa s for 670–1191 km depth or 10^{22} Pa s for 670–1691 km depth. It should be noted that the viscosity jump in the deep mantle has already been inferred from plausible temperature profiles and high-temperature creep in olivine (Ivins *et al*. 1993), postglacial decay times in Canada and Scandinavia (Mitrovica 1996), rotational variations of the Earth (Vermeersen *et al*. 1997) and joint inversions of GIA and convection data sets (Mitrovica & Forte 2004).

On the other hand, Ivins *et al*. (1993) and Mitrovica & Peltier (1993) discussed the zonal secular rates, $\dot{J}_n$ ($n \geq 2$), to explore radial viscosity variations in the lower mantle for varying distance of the step-like viscosity variation interface in the lower mantle. Ivins *et al*. (1993), using GIA ice models of ICE2 (Wu & Peltier 1983) and ICE3G (Tushingham & Peltier 1991) and geopotential zonal secular rates by Cheng *et al*. (1989), pointed out that the zonal secular rates for $n > 2$ provide important constraints on the lower-mantle viscosity and also that the Antarctic melting history significantly influences estimation of lower-mantle viscosity. The most significant difference between the ICE2 and ICE3G is the period of the Antarctic melting; namely, 18–8 kyr BP for the ICE2 and 10–5 kyr BP for the ICE3G. Mitrovica & Peltier (1993) mainly examined the sensitivities of the zonal secular rates to viscosity structure of the mantle based on the ICE3G and indicated that the rates for $n > 5$ are more sensitive to variations in the upper-mantle viscosity. On the other hand, Tosi *et al*. (2005), using the ICE3G and secular rates up to degree 8 (e.g. Cheng *et al*. 1997), inferred the viscosity structure by considering recent melting of the Antarctic and Greenland ice sheets, and obtained a value of the order of 10^{20} Pa s for the upper-mantle viscosity and an average lower-mantle viscosity of 10^{22} Pa s (see also Devoti *et al*. 2001).

These studies suggest that GIA studies using the geopotential zonal secular rates for $n > 2$ provide additional constraints on the mantle viscosity inferred from the $\dot{J}_2$ and RSL changes (Lau *et al*. 2016; Nakada & Okuno 2016), particularly on the lower-mantle viscosity above the mid-lower mantle, if we incorporate the sensitivities of the $\dot{J}_n$ ($n > 2$) to the melting history due to the last deglaciation and also the contribution from recent melting of glaciers and the Greenland and Antarctic ice sheets updated and extended by Vaughan *et al*. (2013). Particularly, it may be important to examine the sensitivities to the Antarctic melting history more systematically than the sensitivity analysis using the ICE2 and ICE3G by Ivins *et al*. (1993). Here, we examine the mantle viscosity and melting history due to the last deglaciation, particularly for the Antarctic ice sheet, by considering the available geopotential zonal secular rates for $n > 2$ (Cheng *et al*. 1989, 1993, 1997; Cazenave *et al*. 1996; Nerem & Klosko 1996; Cox & Chao 2002) and recent melting by Vaughan *et al*. (2013). However, we first point out that the zonal secular rates for $n > 2$ may be available only for the period of 1976–2002 as far as we know, and therefore we cannot discuss the mantle viscosity and GIA ice model based on the method adopted for the $\dot{J}_2$ (Nakada *et al*. 2015) using temporal variations in zonal secular rates for the period of 1976–2011 by Roy & Peltier (2011) and Cheng *et al*. (2013). The paper is organized as follows. In Section 2, we explain the viscosity models and recent and GIA ice models. In Section 3, we examine the sensitivities of the $\dot{J}_n$ to recent and GIA ice models and viscosity model. In Section 4, we infer the viscosity structure based on the results in Section 3 and observationally derived GIA-induced zonal secular rates for $n \leq 6$, and the results obtained in this study are summarized in Section 5.

2 MODEL ADOPTED IN THIS STUDY

2.1 Earth model

We adopt the seismological PREM (Dziewonski & Anderson 1981) for density and elastic constants, as used also in recent studies of Earth's rotation for long mantle convection and short earthquake timescales (Cambiotti *et al*. 2011, 2016), and two typical viscosity models used by Nakada & Okuno (2016). One of the viscosity models is a simple three-layer viscosity model usually used in GIA study (e.g. Wu & Peltier 1984; Lambeck *et al*. 2014) and described by elastic lithospheric thickness (H), upper-mantle viscosity above 670 km depth ($\eta_{\rm um}$) and lower-mantle viscosity ($\eta_{\rm lm}$). The other is a two-layer lower-mantle viscosity model with two layers in the lower mantle. The values for H and $\eta_{\rm um}$ are identical in both viscosity models and adopted values for H and $\eta_{\rm um}$ are: $H = 65$ and 100 km and $\eta_{\rm um} = (1, 2, 3, 4, 5, 7, 10) \times 10^{20}$ Pa s. The lower-mantle viscosities for the simple three-layer viscosity model are (1, 2, 5, 10, 20, 50, 100) $\times$ 10^{21} Pa s, and the lower-mantle viscosity structure for the two-layer lower-mantle viscosity model is characterized by the viscosity from 670 to D km depth, $\eta_{670,D}$, and the viscosity from D to 2891 km depth (CMB), $\eta_{\rm D,2891}$. We adopt 1191 and 1691 km for D-value and examine the GIA-induced $\dot{J}_n$ ($n = 2$–7) for viscosity models with $\eta_{670,\rm D} \leq \eta_{\rm D,2891}$. The results for $\eta_{670,\rm D} > \eta_{\rm D,2891}$ are nearly similar to those for the simple three-layer viscosity model with $\eta_{\rm lm} = \eta_{670,\rm D}$ as obtained for the $\dot{J}_2$ by Nakada & Okuno (2016), although we do not show the results here. The adopted values for $\eta_{\rm D,2891}$ are (10, 20, 50, 100) $\times$ 10^{21} Pa s inferred from recent GIA studies by Nakada & Okuno (2016) and Lau *et al*. (2016). The viscosity model with $\eta_{\rm D,2891} = 10^{23}$ Pa s, for example, is referred to as VL100(D), and this type viscosity model is also referred to as VL(D) here.

2.2 Recent melting model

The melting models for the period of 1900–present are the same as those by Nakada *et al*. (2015) based on an extensive review of the melting of glaciers and the Greenland and Antarctic ice sheets by Vaughan *et al*. (2013) in the IPCC 2013 Report (AR5). The ice models are as follows: MG1 for glaciers, GREENg for glaciers peripheral to the Greenland ice sheet, GREEN for the Greenland ice sheet including the peripheral glaciers and ANT for the Antarctic ice sheet (see Table 1). Each ice model is approximated by several disc loads, and the values of equivalent sea level rise (ESLR) with uncertainty range of 90 per cent for three periods, 1900–1990, 1991–2001 and 2002–2011, are based on the results of tables 4.5 and 4.6 by Vaughan *et al*. (2013). For the MG1, the distribution of glaciers and the height change rate of each disc load are derived from table 4.2 and figs 4.8 and 4.11 in AR5, respectively. The distribution of glaciers for the GREENg describing the melting for 1900–1990 is based on the results of fig. 4.8 in AR5. GREEN ice model is derived from the results of fig. 4.13 in AR5, and has different ESLR values for the periods of 1991–2001 and 2002–2011. The melting model of the Antarctic ice sheet, ANT, is based on the results of fig. 4.14 in AR5 and the disc loads except for the West Antarctica are wholly growing. Here, we examine the impacts of recent Antarctic melting on the $\dot{J}_n$ ($n = 2$–7) based on the ANTw model with melting disc loads limited to the West Antarctica (see fig. 1e in Nakada *et al*. 2015). The ESLR values for adopted melting models are shown in Table 1.

2.3 GIA ice model

We adopt six simplified GIA ice models constructed based on the method by Lambeck (1993) using ice sheet dynamics that the maximum ice thickness at the centre of ice sheet is proportional to the square root of the distance of the ice margin from the centre (Paterson 1971). We assume that the areas of the North American, Fennoscandian, Greenland and Antarctic ice sheets for the LGM at ∼21 kyr BP are the same as those for the ICE5G (Peltier 2004), and those at an arbitrary time are proportional to the ice volume derived from an equivalent sea level (ESL) component of each ice sheet (Nakada *et al*. 2016). The ESL is defined as the change in meltwater volume divided by the surface area of the ocean at the present day. These ice models are inferred from the LGM sea levels at Barbados (Fairbanks 1989; Peltier & Fairbanks 2006) and Bonaparte Gulf in Australia (Yokoyama *et al*. 2000) and their differential value, RSL change at Tahiti (Bard *et al*. 1996; Deschamps *et al*. 2012), and RSL changes after ∼6 kyr BP at Karumba and Halifax Bay in Australia (Chappell *et al*. 1983; Nakada & Lambeck 1989) and the differential value for the sea level highstands at ∼6 kyr BP (Nakada & Okuno 2016). These models have an identical ESL history, $\mathrm{ESL}_{\mathrm{IA}}(t)$ (Total ESL in Fig. 1a), with total ESL component of 127.9 m that is 10 m larger than that for the ICE5G (version 2.1) and identical to the initial model used in the inversion study for far-field sea level data by Lambeck *et al*. (2014), referred to as ANU ice model here.

We adopt IA10, IA20 and IA30 ice models by Nakada & Okuno (2016), in which all ice sheets for IA10, IA20 and IA30 melt synchronously based on the ESL history, $\mathrm{ESL}_{\mathrm{IA}}(t)$. The Antarctic ESL component ($\mathrm{ESL}_{\mathrm{SH}}$) reflects uncertainties of the melting history of the Antarctic ice sheet (e.g. Nakada & Lambeck 1988; Nakada *et al*. 2000; Peltier 2004; Whitehouse *et al*. 2012; Ivins *et al*. 2013; Lambeck *et al*. 2014), and 9.3 m (∼10 m) for the IA10 [similar to the glaciological reconstruction by Whitehouse *et al*. (2012)], 18.7 m (∼20 m) for the IA20 [similar to that for the ANT5 by Nakada *et al*. (2000) and the same as that for the ICE5G] and 28.0 m (∼30 m) for the IA30 (similar to that for the ANU). These ice models are referred to as IA ice models here. The Northern (NH) and Southern Hemisphere (SH) ice models for the IA10, for example, are denoted as IA10(N) and IA10(S), respectively. The ESL histories for these ice models are shown in Fig. 1. In these ice models, the rapid ESL rise at ∼14.5 kyr BP reflects the observed RSL changes at Tahiti (Nakada *et al*. 2016) and the ESL history during the past ∼6 kyr (total ESL rise of ∼2.5 m after 6 kyr BP) is inferred from the observed late-Holocene RSL changes at Karumba and Halifax Bay and their differential sea level highstand at ∼6 kyr BP (Nakada & Lambeck 1989; Nakada & Okuno 2016).

We also discuss the GIA-induced $\dot{J}_n$ based on other three additional ice models, IR10, IR20 and IR30 (referred to as IR ice models here), because the secular rates for $n = 3$–7 are significantly sensitive to the time-dependent melting history of the Antarctic ice sheet as indicated by Ivins *et al*. (1993) using ICE2 and ICE3G ice models. The melting of the Antarctic ice sheet for the ICE5G ($\mathrm{ESL}_{\mathrm{SH}} \sim 20$ m) mainly occurs for 12–6 kyr BP and its ESL history after 12 kyr BP is nearly similar to that for the ANT5 by Nakada *et al*. (2000) inferred from the RSL data in Antarctica [see also ANT4 in Nakada & Lambeck (1989)]. Here, we adopt the ICE5G commonly used in GIA community to construct IR ice models (Fig. 1). The ESL history of the IR20 Antarctic ice model before 6 kyr BP is the same as that for the ICE5G, $\mathrm{ESL}_{5\mathrm{G,A}}(t)$ and the melting ice thicknesses at all sites for the IR20, IR20(S), are proportional to the $\mathrm{ESL}_{5\mathrm{G,A}}(t)$. The total ESL rise after 6 kyr BP for the ICE5G is ∼2.5 m, attributing to the Antarctic melting for 6–5 kyr BP. Here, we adopt the gradual Antarctic melting after 6 kyr BP satisfying the RSL changes at Karumba and Halifax Bay (Fig. 1b). The additional 10.1 m compared to the ESL component of ICE5G (∼118 m) is distributed to the Laurentide, Fennoscandian and Greenland ice sheets by considering their ESL components for the ICE5G, and these ice sheets melt synchronously based on the ESL history of $[\mathrm{ESL}_{\mathrm{IA}}(t) - \mathrm{ESL}_{5\mathrm{G,A}}(t)]$. The melted ice thicknesses at time t for Antarctic IR10 ice model are half for the IR20. Those for the IR30 before 6 kyr BP are one-and-a-half times as large as those for the IR20, and those after 6 kyr BP are the same as those for the IR20. That is, the overarching difference between the two series, IA and IR ice models, is simply the assumed timing history.

3 RESULTS

3.1 $\dot{J}_n$ due to recent melting after ∼1900

We evaluate the $\dot{J}_n$ ($n = 2$–7) due to recent (after ∼1900) melting of glaciers and the Greenland and Antarctic ice sheets, $\dot{J}_n^{\mathrm{RM}}$. The ESLR values are different in three periods of 1900–1990, 1991–2001 and 2002–2011 because of the accelerated melting of glaciers and both ice sheets after ∼1990. The acceleration is also consistent with the observed temporal variations of J_2 (Roy & Peltier 2011; Cheng *et al*. 2013). In this study, we mainly discuss the zonal secular rates for two periods of 1900–1990 and 2002–2011 as was examined by Nakada *et al*. (2015).

Table 1 summarizes the $\dot{J}_n^{\mathrm{RM}}$ for three periods based on the recent melting models and viscosity model with $H = 65$ km, $\eta_{\mathrm{um}} = 4 \times 10^{20}$ and $\eta_{\mathrm{lm}} = 10^{22}$ Pa s. These estimates are almost insensitive to the viscosity model because the Earth response is essentially elastic on these timescales (e.g. Mitrovica & Peltier 1993; Nakada *et al*. 2015). For MG1, GREEN and ANT ice models, the $\dot{J}_n^{\mathrm{RM}}$ value

Table 1. The estimates of the $\dot{J}_n$ ($\times 10^{11}$ yr^{-1}) due to recent melting models ($\dot{J}_n^{\mathrm{RM}}$), MG1 (mountain glaciers), GREENg (peripheral glaciers of the Greenland ice sheet), GREEN (Greenland ice sheet including the peripheral glaciers), ANT (Antarctic ice sheet) and ANTw (West Antarctic ice sheet). These melting models with different ESLR values (mm yr^{-1}) for three periods (1900–1990, 1991–2001 and 2002–2011) are based on recent melting of glaciers and the Greenland and Antarctic ice sheets by Vaughan *et al*. (2013) in the IPCC 2013 Report (see Nakada *et al*. 2015). The numbers within the parentheses for the ANT model show the $\dot{J}_n^{\mathrm{RM}}$ values for the ANTw.

MG1			
Period (ESLR)	1900–1990 (0.54 ± 0.07)	1991–2001 (0.73 ± 0.37)	2002–2011 (0.80 ± 0.37)
$\dot{J}_2^{\mathrm{RM}}$	1.52 ± 0.20	2.06 ± 1.04	2.25 ± 1.04
$\dot{J}_3^{\mathrm{RM}}$	1.01 ± 0.13	1.36 ± 0.69	1.49 ± 0.69
$\dot{J}_4^{\mathrm{RM}}$	0.55 ± 0.07	0.75 ± 0.38	0.82 ± 0.38
$\dot{J}_5^{\mathrm{RM}}$	0.30 ± 0.04	0.41 ± 0.21	0.45 ± 0.21
$\dot{J}_6^{\mathrm{RM}}$	0.28 ± 0.04	0.38 ± 0.19	0.41 ± 0.19
$\dot{J}_7^{\mathrm{RM}}$	0.22 ± 0.03	0.12 ± 0.06	0.13 ± 0.06

Greenland (GREENg for 1900–1990 and GREEN for other periods)			
Period (ESLR)	1900–1990 (0.15 ± 0.05)	1991–2001 (0.09 ± 0.11)	2002–2011 (0.59 ± 0.16)
$\dot{J}_2^{\mathrm{RM}}$	0.62 ± 0.21	0.36 ± 0.44	2.34 ± 0.64
$\dot{J}_3^{\mathrm{RM}}$	0.53 ± 0.18	0.30 ± 0.36	1.94 ± 0.53
$\dot{J}_4^{\mathrm{RM}}$	0.47 ± 0.16	0.25 ± 0.30	1.61 ± 0.44
$\dot{J}_5^{\mathrm{RM}}$	0.29 ± 0.10	0.12 ± 0.15	0.81 ± 0.22
$\dot{J}_6^{\mathrm{RM}}$	0.22 ± 0.07	0.07 ± 0.09	0.46 ± 0.12
$\dot{J}_7^{\mathrm{RM}}$	0.08 ± 0.03	–0.02 ± 0.03	–0.14 ± 0.04

ANT (ANTw)			
Period (ESLR)	1900–1990	1991–2001 (0.08 ± 0.19)	2002–2011 (0.40 ± 0.21)
$\dot{J}_2^{\mathrm{RM}}$		0.34 ± 0.81 (0.35 ± 0.83)	1.71 ± 0.90 (1.76 ± 0.92)
$\dot{J}_3^{\mathrm{RM}}$		–0.32 ± 0.76 (–0.35 ± 0.82)	–1.61 ± 0.85 (–1.73 ± 0.91)
$\dot{J}_4^{\mathrm{RM}}$		0.27 ± 0.64 (0.31 ± 0.74)	1.35 ± 0.71 (1.56 ± 0.82)
$\dot{J}_5^{\mathrm{RM}}$		–0.22 ± 0.51 (–0.27 ± 0.65)	–1.08 ± 0.57 (–1.37 ± 0.72)
$\dot{J}_6^{\mathrm{RM}}$		0.13 ± 0.31 (0.20 ± 0.47)	0.65 ± 0.34 (0.99 ± 0.52)
$\dot{J}_7^{\mathrm{RM}}$		–0.07 ± 0.16 (–0.14 ± 0.33)	–0.33 ± 0.17 (–0.70 ± 0.37)

Total (MG1+GREEN(GREENg)+ANT)			
Period (ESLR)	1900–1990 (0.69 ± 0.12)	1991–2001 (0.90 ± 0.67)	2002–2011 (1.79 ± 0.74)
$\dot{J}_2^{\mathrm{RM}}$	2.10 ± 0.40	2.76 ± 2.27	6.30 ± 2.60
$\dot{J}_3^{\mathrm{RM}}$	1.54 ± 0.31	1.34 ± 1.81	1.82 ± 2.07
$\dot{J}_4^{\mathrm{RM}}$	1.02 ± 0.23	1.27 ± 1.32	3.78 ± 1.53
$\dot{J}_5^{\mathrm{RM}}$	0.59 ± 0.14	0.31 ± 0.87	0.18 ± 1.00
$\dot{J}_6^{\mathrm{RM}}$	0.50 ± 0.11	0.58 ± 0.59	1.52 ± 0.65
$\dot{J}_7^{\mathrm{RM}}$	0.30 ± 0.06	0.03 ± 0.24	–0.33 ± 0.27

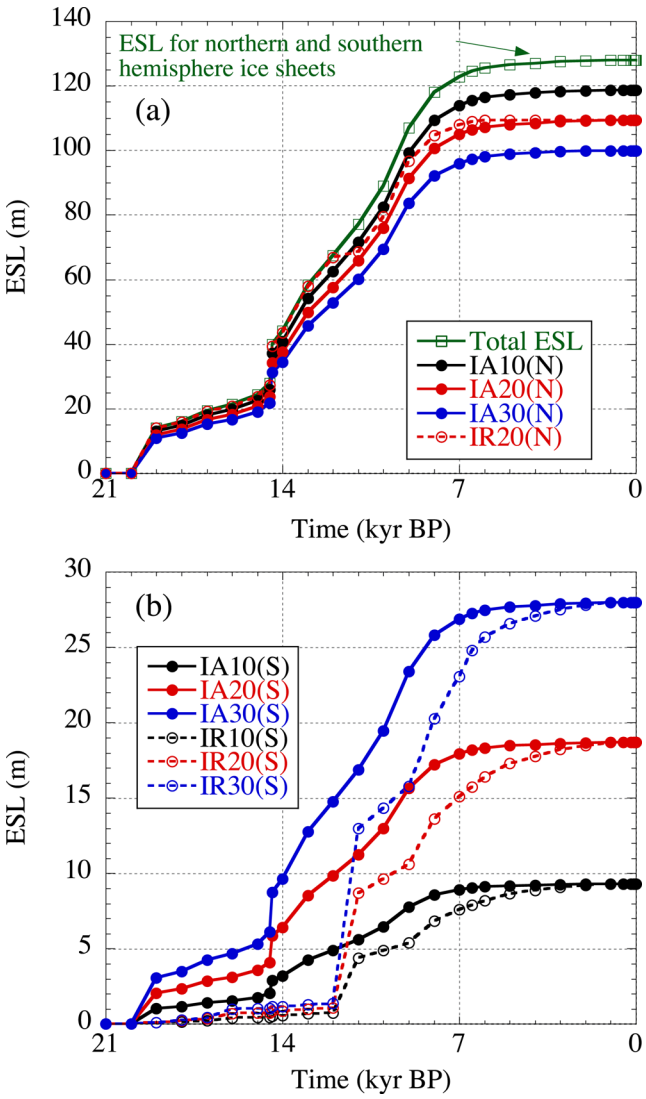

Figure 1. ESL histories as a function of time for GIA ice models adopted here. The ESL history for all IA and IR ice models is denoted by 'Total ESL', and the ESL histories for the Northern and Southern (Antarctic) Hemisphere ice sheets for the IA30 with an Antarctic ESL component of ∼30 m, for example, are shown by IA30(N) and IA30(S), respectively. The ESL is defined here as the change in meltwater volume of all grounded ice divided by the surface of the ocean at the present day.

for each period is proportional to its ESLR value because each ice model has identical melting area for the period from 1900 to 2011. This is not true for the GREENg and GREEN for the Greenland ice sheet and for the ANTw and ANT for the Antarctic ice sheet. The melting areas of the GREENg are different from those for the GREEN, and the melting disc loads for the ANTw are limited to the West Antarctica in contrast to the ANT (Section 2.2). The difference between the $\dot{J}_n^{\mathrm{RM}}$ values for the GREENg and GREEN is negligibly small as inferred from the $\dot{J}_n^{\mathrm{RM}}$ values for 1900–1990 (GREENg) and 1991–2001 (GREEN) and ESLR values for both periods. However, the $\dot{J}_n^{\mathrm{RM}}$ magnitude for the ANTw is larger than that for the ANT for all degree components, which is particularly significant in the rates for $n = 5$, 6 and 7.

We next examine the $\dot{J}_n^{\mathrm{RM}}$ for the total recent melting model: the model corresponding to the Total column in Table 1. An important point in discussing the secular rate is that the secular rates for $n = 3$, 5 and 7 are positive for the Greenland melting models (GREEN and GREENg) and negative for the Antarctic ones (ANT and ANTw) and those for $n = 2$, 4 and 6 are positive for these melting models (Table 1). This is because the odd-degree Legendre function is asymmetric to the equator and the even one is symmetric. For the total recent melting model, consequently, the rates for $n = 2$, 4 and 6 in the period of 2002–2011 are about three times as large as than those for 1900–1990 even for an adoption of the ANTw, while such a significant change is not predicted for the odd zonal rates. The difference between the $\dot{J}_3^{\mathrm{RM}}$ values for three periods is insignificant regardless of the melting models of the ANTw and ANT. However, the secular rates for $n = 5$ and 7 significantly decrease with time because of the dominant contribution from the Antarctic melting, which is particularly clear if we adopt the ANTw.

These degree-dependent characteristics of the $\dot{J}_n^{\mathrm{RM}}$ would be crucial in inferring the GIA-induced $\dot{J}_n$, $\dot{J}_n^{\mathrm{GIA}}$, from geodetically derived geopotential zonal secular rate, $\dot{J}_n^{\mathrm{OBS}}$, and the rate due to recent melting, $\dot{J}_n^{\mathrm{RM}}$. The GIA-induced $\dot{J}_n$ for each degree can be regarded as constant (time-independent) during the past ∼100 yr, since the $\dot{J}_n$ in the postglacial phase after ∼6 kyr BP is determined solely by viscous relaxation processes. That is, if the recent melting models adopted here are wholly correct, then the difference between the $\dot{J}_n^{\mathrm{OBS}}$ values for different periods would arise from accelerated melting after ∼1990 of glaciers and the Greenland and Antarctic ice sheets. In fact, this relation may be almost true for the $\dot{J}_2^{\mathrm{OBS}}$ (Nakada *et al.* 2015).

3.2 GIA-induced $\dot{J}_n$ for the simple three-layer viscosity model

We examine the sensitivities of the GIA-induced $\dot{J}_n$ to the viscosity structure and GIA ice model based on the simple three-layer viscosity model. Fig. 2 shows the contour maps of the zonal secular rates ($n = 2$–7) for IA10, IA20 and IA30 ice models based on the viscosity models with lithospheric thickness (H) of 65 km. We explain the meaning of colour regions in Section 4. The secular rates for $H = 100$ km and the IA20 (red dashed lines) indicate that the rates are almost equal to those for $H = 65$ km, and we therefore examine the rates for $H = 65$ km in the following discussion. The secular rates are negative for $n = 2$–4 and positive for $n = 5$–7 for these ice models in adopted viscosity range. The rates for $n = 2$ are nearly insensitive to GIA ice model as was indicated by Nakada *et al.* (2016). The $\dot{J}_3$ magnitude significantly decreases with increasing ESL component of the Antarctic (SH) ice sheet, $\mathrm{ESL_{SH}}$. For example, the rate at $\eta_{\mathrm{um}} \sim 2 \times 10^{20}$ and $\eta_{\mathrm{lm}} \sim 2 \times 10^{22}$ Pa s is about -2.5×10^{-11} yr^{-1} for the IA10 and -0.1×10^{-11} yr^{-1} for the IA30. The magnitude of the rates for $n = 4$, 5 and 7 increases with increasing $\mathrm{ESL_{SH}}$ value, and that for $n = 6$ decreases with increasing $\mathrm{ESL_{SH}}$ value. The rate for $n = 4$ at $\eta_{\mathrm{um}} \sim 2 \times 10^{20}$ and $\eta_{\mathrm{lm}} \sim 2 \times 10^{22}$ Pa s is about -1.6×10^{-11} yr^{-1} for the IA10 and -3.2×10^{-11} yr^{-1} for the IA30, and that for $n = 5$ is 3.0×10^{-11} yr^{-1} for the IA10 and 4.4×10^{-11} yr^{-1} for the IA30. Fig. 3 shows the secular rates for IR10, IR20 and IR30 ice models. The rate for $n = 2$ is also less sensitive to the ice model. In the $\dot{J}_3^{\mathrm{GIA}}$, the difference between the rates for the IR10 and IR30 is larger than that for the IA10 and IA30, and also the rates for the IR30 are positive in contrast to negative for the IA30. The rate at $\eta_{\mathrm{um}} \sim 2 \times 10^{20}$ and $\eta_{\mathrm{lm}} \sim 2 \times 10^{22}$ Pa s is about -2.0×10^{-11} yr^{-1} for the IR10 and 1.0×10^{-11} yr^{-1} for the IR30. The sensitivities of the rates for $n = 3$–7 are wholly similar to those for IA ice models. Thus, the rates for $n = 3$–7 are sensitive to GIA ice model as well as the viscosity structure.

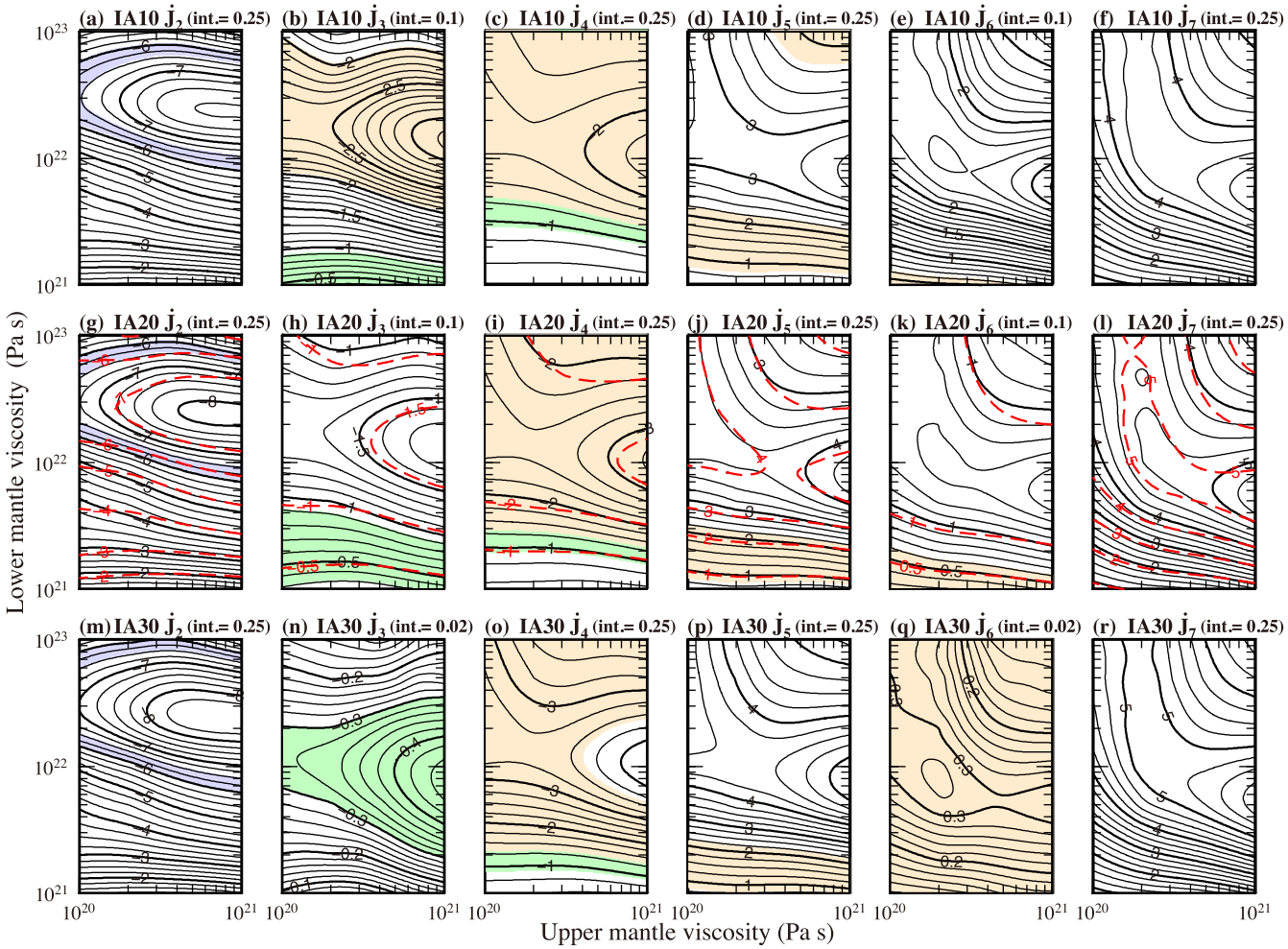

Figure 2. Contour maps of GIA-induced $\dot{J}_n$ ($2 \le n \le 7$) based on IA10, IA20 and IA30 ice models and simple three-layer viscosity models with lithospheric thickness (H) of 65 km, and those for the IA20 and $H = 100$ km. Permissible viscosity ranges satisfying observationally derived $\dot{J}_2$ of –(6.0–6.5) $\times 10^{-11}$ yr^{-1} (Nakada *et al*. 2015) is shown by blue colour, and the regions shown by orange and green colours indicate the permissible viscosity ranges based on the GIA-induced zonal secular rates using the geopotential zonal secular rates by Cheng *et al*. (1997) and Cox & Chao (2002), respectively (see Table 2). The comparison between the observationally derived and predicted zonal secular rates is discussed in Section 4.

To clearly understand the sensitivity of the GIA-induced $\dot{J}_n$ ($n = 2$–7) to ice and viscosity models, we examine the secular rates for the NH and SH ice models in more detail based on the viscosity models with upper-mantle viscosity ($\eta_{\rm um}$) of 2×10^{20} Pa s and lithospheric thickness (H) of 65 km. The essential points for the sensitivity do not change even if we adopt $H = 100$ km or other upper-mantle viscosities as inferred from the rates predicted for the IA20 shown in Fig. 2. Figs 4(a) and (b) show the $\dot{J}_2^{\rm GIA}$ as a function of lower-mantle viscosity ($\eta_{\rm lm}$) for IA and IR ice models, respectively. For the NH and SH ice models, the rates are negative in a range of $\eta_{\rm lm} = (1-100) \times 10^{21}$ Pa s and the magnitude is proportional to the ESL component. The relation between the $\dot{J}_2^{\rm GIA}$ magnitude and ESL component is true for other zonal secular rates. Here, we examine the sensitivity to GIA ice model based on the predicted rates at $\eta_{\rm lm} = 2 \times 10^{22}$ Pa s. The value is -6.9×10^{-11} yr^{-1} for the IA10 and -7.4×10^{-11} yr^{-1} for the IA30. Those for the NH ice models of IA10(N) ($\rm ESL_{NH} \sim 120$ m) and IA30(N) ($\rm ESL_{NH} \sim 100$ m) are -6.1×10^{-11} and -5.1×10^{-11} yr^{-1}, respectively. The contribution from the SH ice sheet is -0.7×10^{-11} yr^{-1} for the IA10(S) ($\rm ESL_{SH} \sim 10$ m) and -2.2×10^{-11} yr^{-1} for the IA30(S) ($\rm ESL_{SH} \sim 30$ m).

Fig. 4(b) shows the $\dot{J}_2^{\rm GIA}$ for IR ice models. The rate at $\eta_{\rm lm} = 2 \times 10^{22}$ Pa s is -7.0×10^{-11} yr^{-1} for the IR10 and -7.9×10^{-11} yr^{-1} for the IR30. The rate is -5.8×10^{-11} yr^{-1} for the IR10(N) and -4.4×10^{-11} yr^{-1} for the IR30(N), and those for the IR10(S) and IR30(S) are -1.1×10^{-11} and -3.4×10^{-11} yr^{-1}, respectively. The comparison between the secular rates for IA and IR Antarctic ice models with an identical ESL component clearly indicates that the magnitude for the IR is (1.5–1.6) times as large as that for the IA. This would be attributed to the melting period of the Antarctic ice sheet that the onset time for the melting of the IA is 21 kyr BP, while that for the IR is 12 kyr BP (Fig. 1). For the NH IA and IR ice models with an identical ESL component, for example, for the IA30(N) and IR30(N), the $\dot{J}_2^{\rm GIA}$ magnitude for the IR is smaller than that for the IA. As a consequence of these sensitivities of the $\dot{J}_2^{\rm GIA}$ to both hemisphere ice models, the rates at $\eta_{\rm lm} = 2 \times 10^{22}$ Pa s are nearly similar for IA and IR ice models with identical ESL components for both hemisphere ice sheets. This is true for the GIA-induced $\dot{J}_2$ predicted for viscosity models with $\eta_{\rm lm} = (1-100) \times 10^{21}$ Pa s.

Figs 4(c) and (d) show the GIA-induced $\dot{J}_3$ as a function of lower-mantle viscosity for IA and IR ice models, respectively. The secular rates in a range of $\eta_{\rm lm} = (1-100) \times 10^{21}$ Pa s are negative

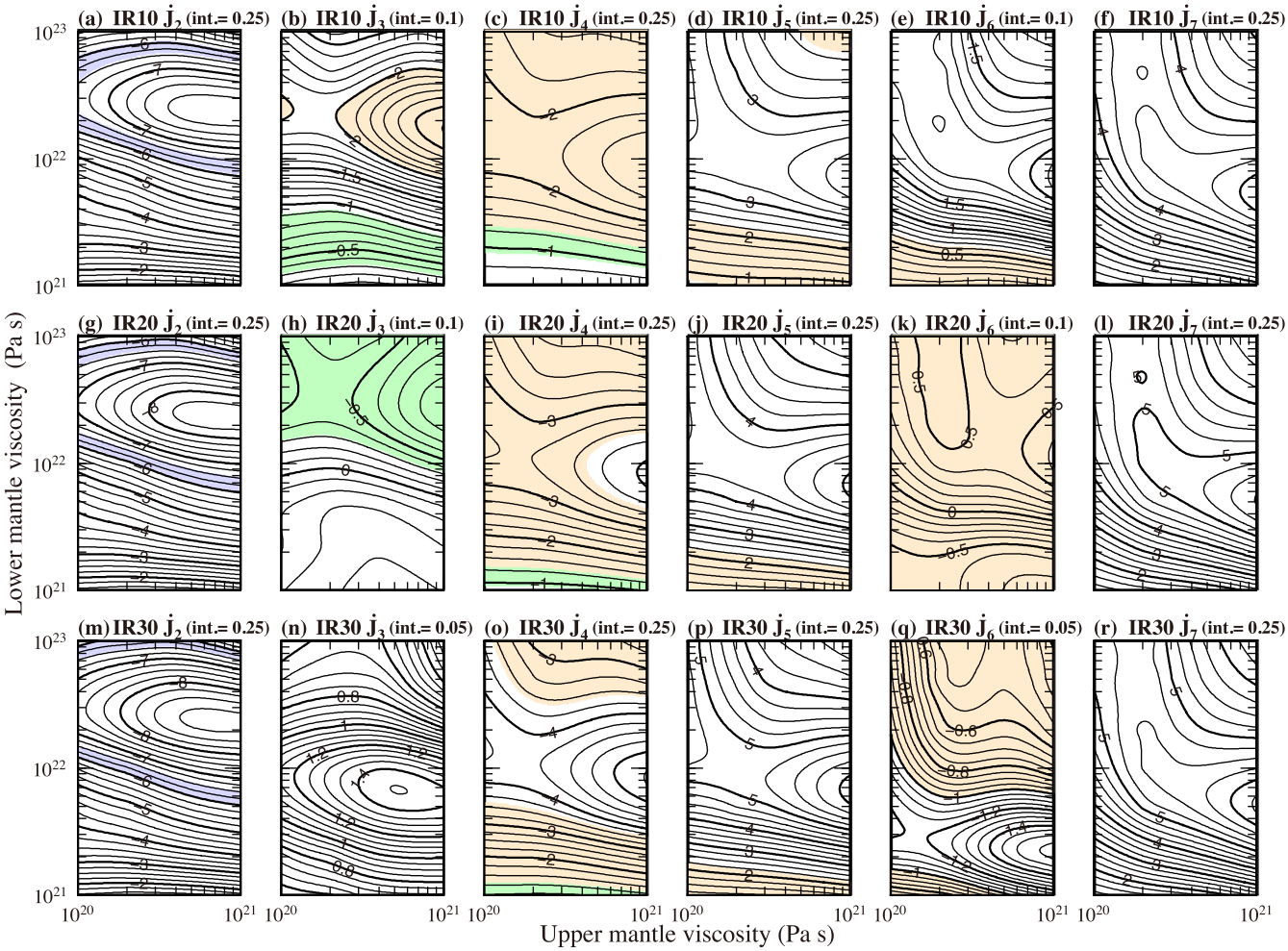

Figure 3. As in Fig. 2, except for IR10, IR20 and IR30 ice models.

for all NH ice models and positive for all SH ones. This relation is different from that for the $\dot{J}_2^{\rm GIA}$, which is attributed to the fact that the degree-three Legendre function is asymmetric to the equator and the degree-two is symmetric. Here, we examine the sensitivity of the $\dot{J}_3^{\rm GIA}$ to GIA ice model from a viewpoint of its sensitivity to ESL component and melting period of the Antarctic ice sheet. We first discuss the sensitivity to the ESL component ($\rm ESL_{SH}$) based on the rates at $\eta_{\rm lm} = 2 \times 10^{22}$ Pa s. The values for the IA10 and IA30 are about -2.5×10^{-11} and -0.3×10^{-11} $\rm yr^{-1}$, respectively, and the difference is $\sim 2.2 \times 10^{-11}$ $\rm yr^{-1}$. The difference between the rates for the IA10(N) and IA30(N) is 0.6×10^{-11} $\rm yr^{-1}$ and that for the IA10(S) ($\rm ESL_{SH} \sim 10$ m) and IA30(S) ($\rm ESL_{SH} \sim 30$ m) is 1.7×10^{-11} $\rm yr^{-1}$. That is, change in $\dot{J}_3^{\rm GIA}$ magnitude for the IA10 and IA30 is mainly attributable to the Antarctic ESL component. This is true for the secular rate for IR ice models (Fig. 4d). That is, the rate at $\eta_{\rm lm} = 2 \times 10^{22}$ Pa s is -2.0×10^{-11} $\rm yr^{-1}$ for the IR10 and 1.0×10^{-11} $\rm yr^{-1}$ for the IR30, and the NH and SH contributions for the difference (3.0×10^{-11} $\rm yr^{-1}$) are about 0.6×10^{-11} and 2.3×10^{-11} $\rm yr^{-1}$, respectively. These sensitivities inferred from the secular rates for IA and IR ice models indicate that the Antarctic ESL component plays an important role on the GIA-induced $\dot{J}_3$.

We next discuss the sensitivity of the $\dot{J}_3^{\rm GIA}$ to the melting period of the Antarctic ice sheet (Fig. 1). Fig. 4(c) indicates that the secular rates for NH ice models at a given $\eta_{\rm lm}$ value change insignificantly for IA10, IA20 and IA30 ice models, and the difference between the rates for these ice models is at most $\sim 0.6 \times 10^{-11}$ $\rm yr^{-1}$. This is true for IR ice models (Fig. 4d). Moreover, the rate at a given $\eta_{\rm lm}$ is nearly similar for the NH IA and IR ice models with an identical $\rm ESL_{NH}$ model [see, e.g. the rates for the IA30(N) and IR30(N)]. However, there is a significant difference between the rates for the Antarctic ice models with an identical ESL component. For example, the maximum $\dot{J}_3^{\rm GIA}$ value is $\sim 2.6 \times 10^{-11}$ $\rm yr^{-1}$ for the IA30(S) and $\sim 3.6 \times 10^{-11}$ $\rm yr^{-1}$ for the IR30(S), and consequently, the secular rates are positive for the IR30, while negative for the IA30. We also note that the rates for the IA30 are nearly similar to those for the IR20; namely, 0 to -0.3×10^{-11} $\rm yr^{-1}$ for the IA30 and -0.4×10^{-11} to 0.3×10^{-11} $\rm yr^{-1}$ for the IR20. This is caused by the viscous response to the melting of the Antarctic ice sheet that the secular rates for the IA30(S) ($\rm ESL_{SH} \sim 30$ m) are nearly equal to those for the IR20(S) ($\rm ESL_{SH} \sim 20$ m), suggesting that the contribution from the melting before $\sim$12 kyr BP for the IA30(S) is significantly smaller than that after $\sim$12 kyr BP (see Fig. 1). That is, the melting period of the Antarctic ice sheet plays an important role on the GIA-induced $\dot{J}_3$ as was indicated by Ivins *et al.* (1993) using the ICE2 and ICE3G.

We examine the GIA-induced $\dot{J}_4$. Figs 4(e) and (f) show the zonal secular rates for IA and IR ice models, respectively. The NH and SH contributions are negative for all ice models, which is the same as that for the $\dot{J}_2^{\rm GIA}$. The most significant difference between the predicted zonal secular rates for $n = 2$ and 4 is that the NH

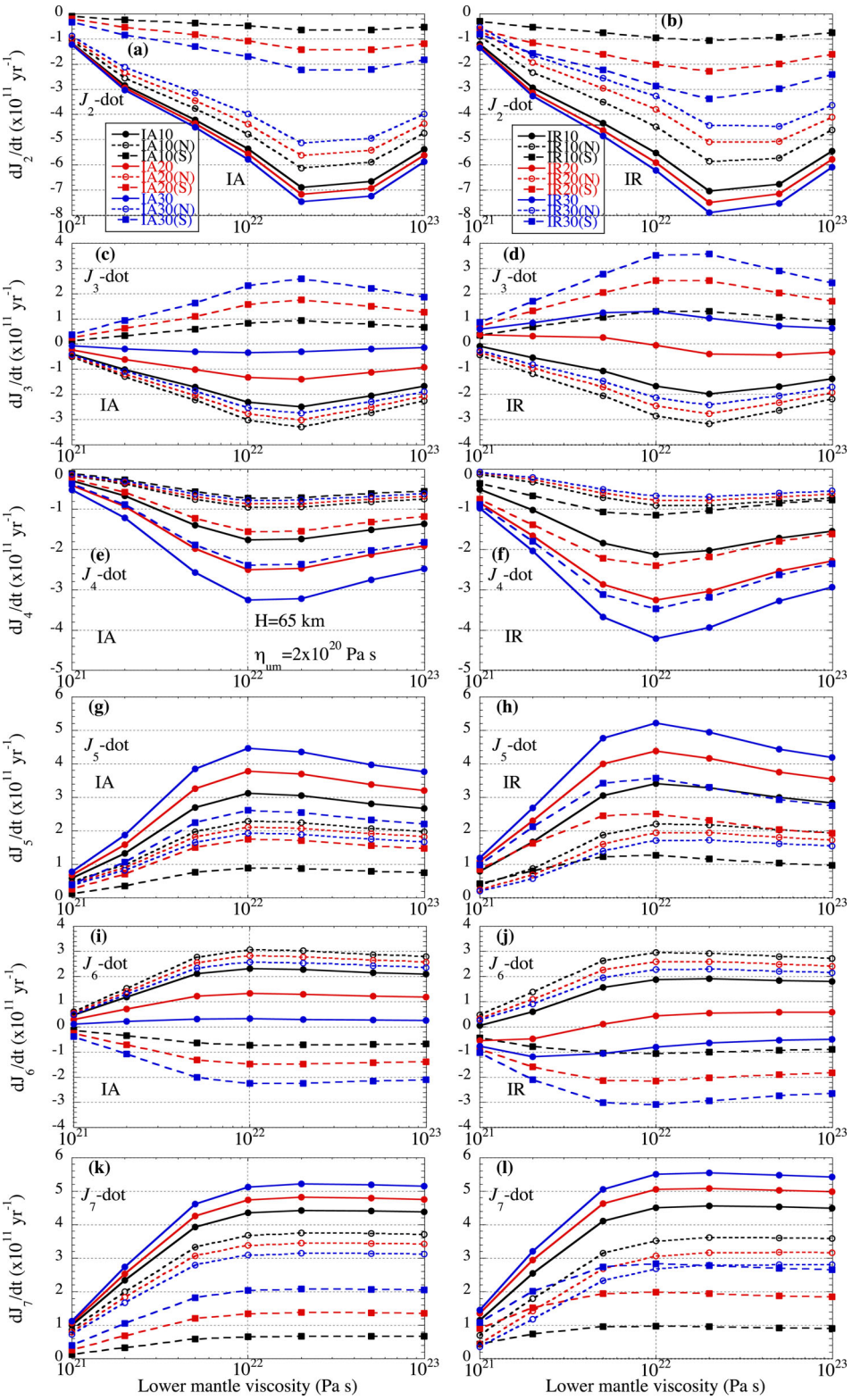

Figure 4. GIA-induced $\dot{J}_n (2 \leq n \leq 7)$ for IA10, IA20, IA30, IR10, IR20 and IR30 ice models and their Northern and Southern Hemisphere ice models based on the simple three-layer viscosity models with upper-mantle viscosity ($\eta_{\rm um}$) of 2×10^{20} Pa s and lithospheric thickness (H) of 65 km.

contribution is significantly small compared with the SH one in the $\dot{J}_4^{\rm GIA}$. For all NH ice models, the $\dot{J}_4^{\rm GIA}$ magnitude is less than 1.0×10^{-11} yr^{-1} and also the maximum difference between the predicted rates at a given $\eta_{\rm lm}$ is at most 0.2×10^{-11} yr^{-1}. That is, the sensitivity of the secular rate to GIA ice model is mainly determined by the response to the melting of the Antarctic ice sheet. For example, the rates at $\eta_{\rm lm} = 2 \times 10^{22}$ Pa s are -0.9×10^{-11} yr^{-1} for the IA20(N), -1.5×10^{-11} yr^{-1} for the IA20(S) and -2.4×10^{-11} yr^{-1} for the IA20 (Fig. 4e). This trend is more clear for IR ice models; namely, -0.8×10^{-11} yr^{-1} for the IR20(N),

-2.2×10^{-11} yr^{-1} for the IR20(S) and -3.1×10^{-11} yr^{-1} for the IR20 (Fig. 4f). Also, the secular rates predicted for the IA30 are nearly similar to those for the IR20 as was obtained for the $\dot{J}_3^{\rm GIA}$, which is explained by considering the GIA-induced $\dot{J}_4$ values for the IA30(S) and IR20(S).

The GIA-induced $\dot{J}_5$ values for IA and IR ice models are shown in Figs 4(g) and (h), respectively. The NH and SH contributions are positive for all ice models. The secular rate for NH ice models is less sensitive to GIA ice model and the rates are nearly similar for NH ice models with an identical NH ESL component ($\rm ESL_{NH}$), for example, for the IA30(N) and IR30(N). Also, the difference between the rates at a given $\eta_{\rm lm}$ for NH ice models is less than 0.5×10^{-11} yr^{-1}. That is, the sensitivity of the rate to GIA ice model is mainly determined by the response to the melting of the Antarctic ice sheet. Also, the rates for the IA30 are almost similar to those for the IR20 as was obtained for the $\dot{J}_3^{\rm GIA}$ and $\dot{J}_4^{\rm GIA}$.

The $\dot{J}_6^{\rm GIA}$ values for IA and IR ice models are shown in Figs 4(i) and (j), respectively. The rates for NH ice models are positive and those for SH ones are negative. The sensitivities to GIA ice model is nearly the same as those for the $\dot{J}_5^{\rm GIA}$. Figs 4(k) and (l) show the GIA-induced $\dot{J}_7$ for IA and IR ice models, respectively. The NH and SH contributions are positive for all ice models. Although the sensitivities are wholly the same as those for the $\dot{J}_5^{\rm GIA}$, the $\dot{J}_7^{\rm GIA}$ values for both hemisphere ice models equally contribute to the rates for IA and IR ice models as was derived from the secular rate for $n = 6$.

3.3 GIA-induced $\dot{J}_n$ for the two-layer lower-mantle viscosity model

The GIA-induced $\dot{J}_2$ for the two-layer lower-mantle viscosity model, VL(D), has been discussed by Nakada & Okuno (2016) in detail, and we therefore examine the $\dot{J}_n^{\rm GIA}$ for $n = 3$–6 here. Although we examine the secular rates based on the viscosity models with $\eta_{\rm um} = 2 \times 10^{20}$ Pa s, the sensitivity to $\eta_{670,\rm D}$ value (viscosity from 670 to D km depth) for a fixed $\eta_{\rm D,2891}$ value (viscosity from D to 2891 km depth) is generally applicable to those for the upper-mantle viscosities of $(1-10) \times 10^{20}$ Pa s. The sensitivity to $\eta_{670,\rm D}$ value is also applicable to that for the secular rate of $n = 2$ (Nakada & Okuno 2016).

Fig. 5 shows the GIA-induced $\dot{J}_3$ values for IA10, IA20, IA30 and IR20 ice models based on the VL viscosity model as a function of $\eta_{670,\rm D}$, and those for the simple three-layer viscosity model (denoted by 3L in Fig. 5) as a function of lower-mantle viscosity ($\eta_{\rm lm}$). We discuss the $\dot{J}_3^{\rm GIA}$ for the IA10 (Fig. 5a) in detail. The $\dot{J}_3^{\rm GIA}$ magnitude for the simple three-layer viscosity model increases with decreasing lower-mantle viscosity in a range of $2 \times 10^{22} \le \eta_{\rm lm} \le 10^{23}$ Pa s. The increase of $\dot{J}_3^{\rm GIA}$ magnitude with decreasing $\eta_{670,1191}$ for the VL100(1191) and $\eta_{670,1691}$ for the VL100(1691) is explained by reference to the predicted rates at $\eta_{\rm lm} = 2 \times 10^{22}$ and 10^{23} Pa s for the simple three-layer viscosity model. That is, the effective lower-mantle viscosity for the VL100(1191) and VL100(1691) (10^{23} Pa s below 1191 and 1691 km depth, respectively) decreases with decreasing $\eta_{670,1191}$ and $\eta_{670,1691}$, and consequently change in $\dot{J}_3^{\rm GIA}$ magnitude with decreasing $\eta_{670,1191}$ ($\eta_{670,1691}$) is expected to take a similar trend of the secular rate for the simple three-layer viscosity model that the magnitude increases with decreasing $\eta_{\rm lm}$ from 10^{23} to 2×10^{22} Pa s. The magnitude for the VL20(1191) and VL20(1691) (also VL10) decreases with decreasing $\eta_{670,1191}$ and $\eta_{670,1691}$, which is also explained if we consider the rates for $\eta_{\rm lm} \le 2 \times 10^{22}$ Pa s in the simple three-layer viscosity model.

The $\dot{J}_3^{\rm GIA}$ magnitude for $\eta_{670,1691} \le 2 \times 10^{21}$ Pa s in VL100(1691) viscosity model is, however, inconsistent with the trend for the VL100(1191) discussed above, and the magnitude decreases with decreasing $\eta_{670,1691}$. The effective lower-mantle viscosity for such a viscosity model may be smaller than 2×10^{22} Pa s for the simple three-layer viscosity model, and consequently change in $\dot{J}_3^{\rm GIA}$ magnitude would take a trend of the rate for the simple three-layer viscosity model that the magnitude decreases with decreasing $\eta_{\rm lm}$ for $\eta_{\rm lm} \le 2 \times 10^{22}$ Pa s. The sensitivity of the $\dot{J}_3^{\rm GIA}$ to the viscosity of $\eta_{670,\rm D}$ for a fixed viscosity of $\eta_{\rm D,2891}$, which is tightly related to the peak position of the secular rate for the simple three-layer viscosity model, is the same as that for the $\dot{J}_2^{\rm GIA}$ in Nakada & Okuno (2016), and also applicable to the zonal secular rates for $n = 3$–6 regardless of GIA ice models of IA10, IA20, IA30 and IR20 [see results for $n = 4$ (Fig. 6), $n = 5$ (Fig. 7) and $n = 6$ (Fig. 8).

We next examine change in $\dot{J}_n^{\rm GIA}$ depending on $\eta_{670,\rm D}$ and $\eta_{\rm D,2891}$ values by comparing the zonal secular rates predicted for the two-layer lower-mantle viscosity model and simple three-layer viscosity model. This would be useful to infer the two-layer lower-mantle viscosity structure from the GIA-induced $\dot{J}_n$ for $n > 2$. Here, we discuss the $\dot{J}_3^{\rm GIA}$ for the IA10 (Fig. 5a) in detail. The rate for the VL100(1191) in Fig. 5(a) indicates that the rate decreases with decreasing $\eta_{670,1191}$ and the values at $\eta_{670,1191} = 10^{23}$ and 10^{21} Pa s are about -1.7×10^{-11} and -2.2×10^{-11} yr^{-1}, respectively, in which the rate at $\eta_{670,1191} = 10^{21}$ Pa s is nearly equal to the value at $\eta_{\rm lm} = 2 \times 10^{22}$ Pa s for the simple three-layer viscosity model. That is, the predicted rate at $\eta_{\rm lm} = 2 \times 10^{22}$ Pa s for the simple three-layer viscosity model is also predicted for the two-layer lower-mantle viscosity model with $\eta_{670,1191} = 10^{21}$ and $\eta_{1191,2891} = 10^{23}$ Pa s. Similar result is also obtained for the VL50. On the other hand, the rate for VL20 (1691) increases with decreasing $\eta_{670,1691}$ and the rate at $\eta_{670,1691} = 10^{21}$ Pa s is about -1.7×10^{-11} yr^{-1}, which is nearly equal to that for $\eta_{\rm lm} = 10^{23}$ Pa s for the simple three-layer viscosity model. However, the rates for VL20 (1191) are nearly constant in a range of $\eta_{670,1191} \le 2 \times 10^{22}$ Pa s, suggesting that the $\dot{J}_3^{\rm GIA}$ for the two-layer lower-mantle viscosity model with $\eta_{1191,2891} = 2 \times 10^{22}$ Pa s is almost insensitive to the viscosity for 670–1191 km depth, $\eta_{670,1191}$. The result for the VL20 is also applicable to that for the VL10. The sensitivity of the $\dot{J}_3^{\rm GIA}$ based on the results for the IA10 is generally applicable to that for the secular rates predicted for ice models of IA20 (Fig. 5b), IA30 (Fig. 5c) and IR20 (Fig. 5d). In Section 4, we discuss the viscosity structure by comparing the GIA-induced zonal secular rates predicted for viscosity and GIA ice models and observationally derived $\dot{J}_n^{\rm GIA}$ for $n = 3$–6.

4 DISCUSSION

Geopotential zonal secular rates of J_n for $n \ge 2$ derived from SLR observations provide important constraints on the mantle viscosity, GIA ice model and recent melting of glaciers and the Greenland and Antarctic ice sheets (e.g. Ivins *et al*. 1993; Mitrovica & Peltier 1993; Devoti *et al*. 2001; Tosi *et al*. 2005). For example, Ivins *et al*. (1993), using two GIA ice models of ICE2 and ICE3G, pointed out that the Antarctic melting history significantly influences estimation of lower-mantle viscosity. It is, however, crucial to discuss these quantities by taking into account the accuracy of geodetically derived geopotential zonal secular rate, $\dot{J}_n^{\rm OBS}$, particularly for the rates of $n > 2$ (e.g. Cheng *et al*. 1997). The accuracy of $\dot{J}_n^{\rm OBS}$ depends on several factors such as the orbital geometry and data span of individual satellite and also aliasing effect from the higher degree (Cheng *et al*. 1997). Cheng *et al*. (1997), using SLR data from the

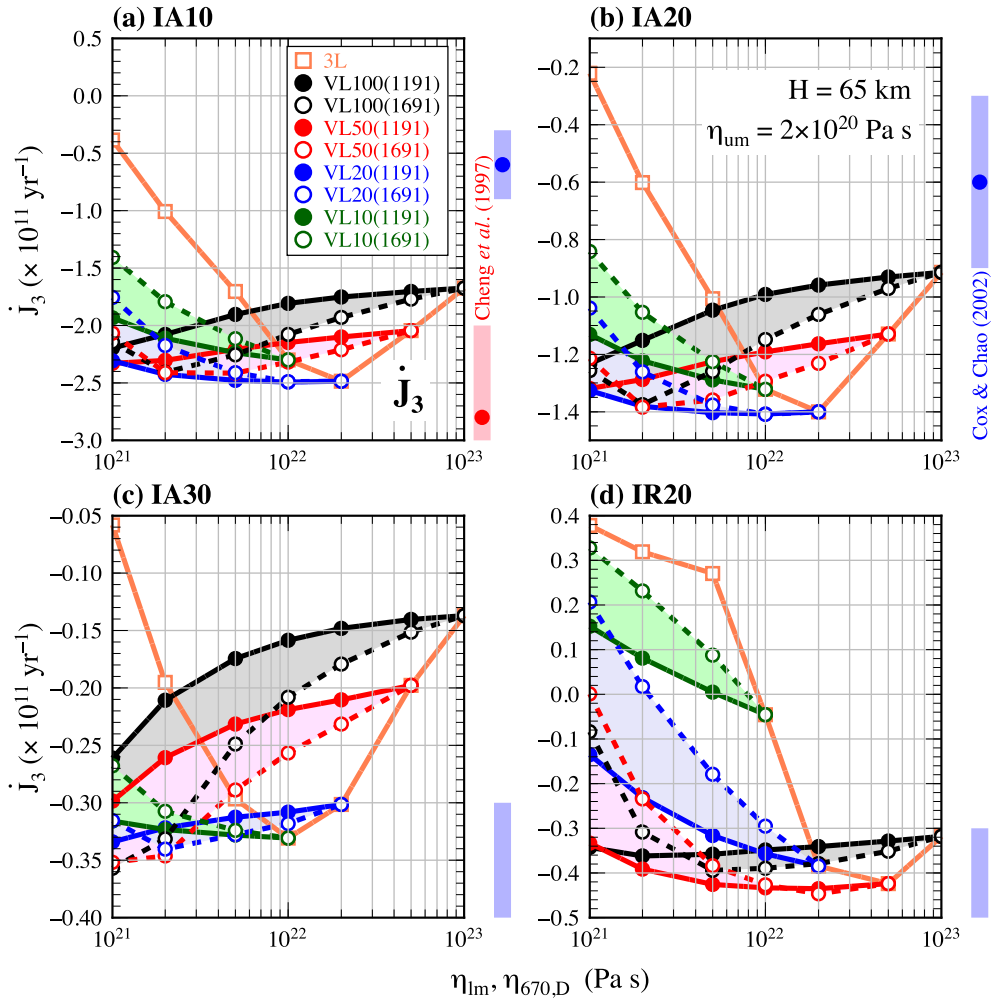

Figure 5. GIA-induced $\dot{J}_3$ based on IA10, IA20, IA30 and IR20 ice models and VL viscosity models with upper-mantle viscosity (η_{um}) of 2×10^{20} Pa s and lithospheric thickness (H) of 65 km: (a) results for the IA10 based on the simple three-layer viscosity model (denoted by 3 L) as a function of lower-mantle viscosity (η_{lm}) and two-layer lower-mantle viscosity model as a function of viscosity $\eta_{670,D}$ for 670-D km depth (D = 1191 and 1691 km), (b) for the IA20, (c) for the IA30 and (d) for the IR20.The viscosities from D to 2891 km depth ($\eta_{D,2891}$) are 10^{23}, 5×10^{22}, 2×10^{22} and 10^{22} Pa s for VL100, VL50, VL20 and VL10 viscosity models, respectively. GIA-induced zonal secular rates based on the geopotential zonal secular rates by Cheng *et al.* (1997) and Cox & Chao (2002) are also shown on the right-hand side of each figure. The comparison between the observationally derived and predicted zonal secular rates is discussed in Section 4.

eight geodetic satellites, concluded that the odd zonal secular rates are less observable than even zonal ones due to weakness in the orbital geometry. They also indicated that multisatellite SLR data sets are required to improve the determination of the zonal secular rate and also separation from the higher degree $\dot{J}_n$, but further efforts are required to improve the determination of the zonal secular rates even for multisatellite data sets. They also stated that the accuracy of the estimates of the zonal secular rates determined from long time-series of multisatellite SLR data has been difficult to verify, and only $\dot{J}_2$ has been evaluated with confidence. By considering these points, we discuss the mantle viscosity and GIA ice model based on the geopotential zonal secular rates for $n = 3$–6 using eight geodetic satellite observations by Cheng *et al.* (1997) and the rates for $n = 3$ and 4 using 10 satellite ones by Cox & Chao (2002). In particular, it may be important to discuss these quantities based on negative $\dot{J}_3$ estimate of $-(1.3 \pm 0.5) \times 10^{-11}$ yr^{-1} (Cheng *et al.* 1997) and positive one of $\sim 0.9 \times 10^{-11}$ yr^{-1} (Cox & Chao 2002) if we consider uncertainties for the determination of the odd zonal secular rate. We shortly comment about the geopotential zonal rates for $n = 3$ and 4 by Cox & Chao (2002). The estimate of $\sim 0.9 \times 10^{-11}$ yr^{-1} for $n = 3$ seems to be constant for the period of 1979–2002, but the rate of $n = 4$ for 1979–1992 seems to be similar to that by Cheng *et al.* (1997) [see supplemental figs 2 and 4 in Cox & Chao (2002)]. Essential points for the following discussion about the mantle viscosity and GIA ice model change insignificantly even if we adopt other available geopotential zonal secular rates (Cheng *et al.* 1989; Cazenave *et al.* 1996; Nerem & Klosko 1996) [see compilations by Cheng *et al.* (1997) and Tosi *et al.* (2005)].

The geopotential zonal secular rates by Cheng *et al.* (1997) and Cox & Chao (2002) are based on the SLR data sets from 1976 to 1995 and 1979 to 2002, respectively. The GIA-induced $\dot{J}_n$, $\dot{J}_n^{\mathrm{GIA}}$, would be estimated by subtracting the rate due to recent melting of glaciers and the Greenland and Antarctic ice sheets, $\dot{J}_n^{\mathrm{RM}}$, from the geopotential zonal secular rate, $\dot{J}_n^{\mathrm{OBS}}$. The mean values of the recent melting contribution for $n = 3$–6 change insignificantly for the period of 1900–2001 (Table 1), and we therefore adopt the recent melting contribution for the period of 1900–1990 here. Table 2 shows the estimates of $\dot{J}_n^{\mathrm{GIA}}$ and the lumped-sum values for $\dot{J}_3$ and $\dot{J}_5$ using the SLR data for a single satellite by Cheng *et al.* (1997) and Devoti *et al.* (2001). The permissible viscosity solution for the

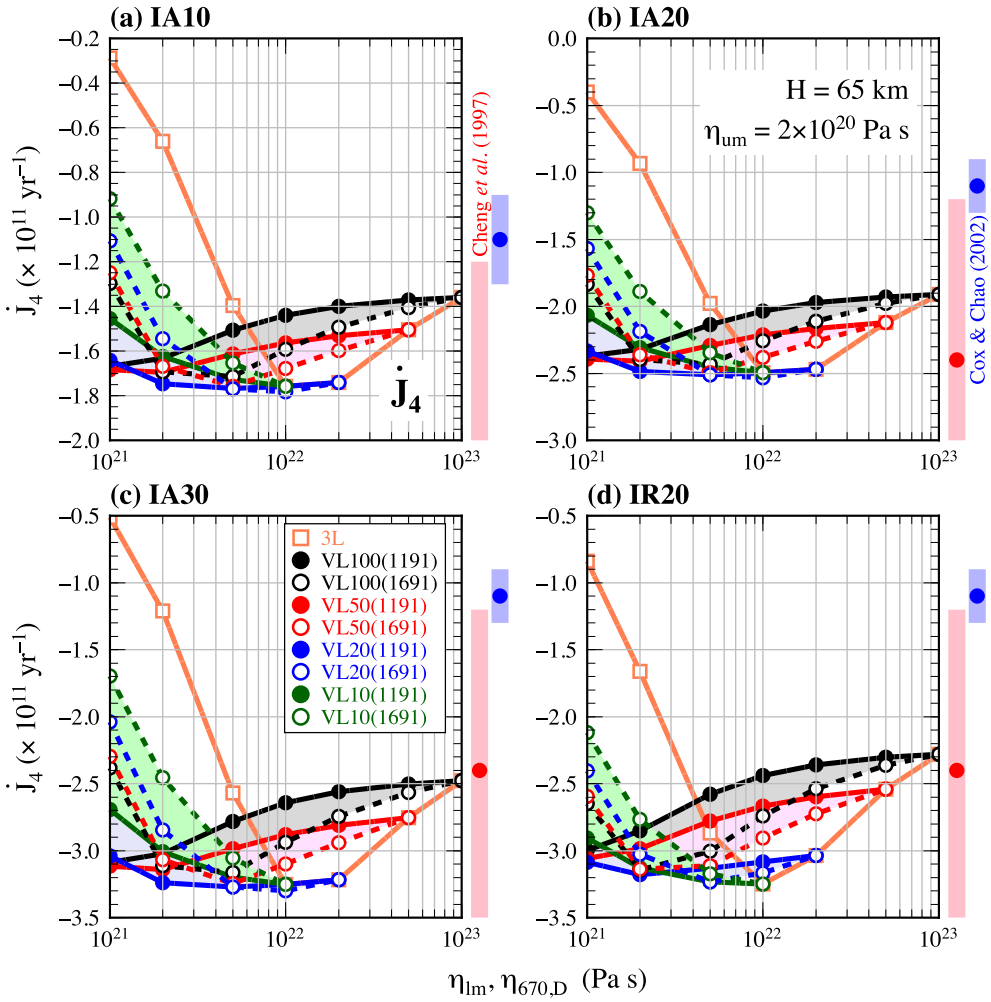

Figure 6. As in Fig. 5, except for the GIA-induced $\dot{J}_4$.

simple three-layer viscosity model inferred from the GIA-induced $\dot{J}_2$ of –(6.0–6.5) × 10^{-11} yr^{-1} (regions shown by blue colour in Figs 2 and 3), which is nearly insensitive to the GIA ice model, was discussed by Nakada *et al.* (2015) in detail.

In the last column of Table 2, we also show the $\dot{J}_n^{GIA}$ for the recent melting rate (ESLR) of (0.95 ± 0.17) mm yr^{-1} to discuss the effect of uncertainties of the melting rate for the period of 1900–1990 on the inferred mantle viscosity. We explain this point by considering the GIA-induced $\dot{J}_2$of –(6.0–6.5) × 10^{-11} yr^{-1} (Nakada *et al.* 2015) inferred from the observationally derived $\dot{J}_2$, $\dot{J}_2^{OBS}$, for the periods of 1976–1990 and 2002–2011 (Roy & Peltier 2011; Cheng *et al.* 2013) and the melting rates for both periods (Vaughan *et al.* 2013). The recent melting component of the zonal secular rate, $\dot{J}_2^{RM}$, due to the melting rate of (0.69 ± 0.12) mm yr^{-1} for 1900–1990 is (2.1 ± 0.4) × 10^{-11} yr^{-1} (Table 1), and the $\dot{J}_2^{GIA}$ is estimated to be –(5.8 ± 0.5) × 10^{-11} yr^{-1} for the $\dot{J}_2^{OBS}$ of –(3.7 ± 0.1) × 10^{-11} yr^{-1}. For the period of 2002–2011, $\dot{J}_2^{RM}$ and $\dot{J}_2^{GIA}$ values are estimated to be (6.3 ± 2.6) × 10^{-11} (Table 1) and –(6.6 ± 2.7) × 10^{-11} yr^{-1}, respectively, based on the observationally derived $\dot{J}_2^{OBS}$ of –(0.3 ± 0.1) × 10^{-11} yr^{-1}. Then, Nakada *et al.* (2015) adopted –(6.0–6.5) × 10^{-11} yr^{-1} for the $\dot{J}_2^{GIA}$ to infer the mantle viscosity (see also Mitrovica *et al.* 2015). If we adopt the $\dot{J}_2^{GIA}$ of –6.6 × 10^{-11} yr^{-1} for the period of 1900–1990, then we obtain –2.9 × 10^{-11} yr^{-1} for the $\dot{J}_2^{RM}$ and the melting rate of 0.69 × 2.9/2.1 ∼ 0.95 mm yr^{-1}. In this study, we discuss the effect of uncertainties of the recent melting rate for the period of 1900–1990 on the inferred mantle viscosity by examining the differences between the viscosity solutions inferred from the $\dot{J}_n^{GIA}$ ($n > 2$) for the melting rates of (0.69 ± 0.12) and (0.95 ± 0.17) mm yr^{-1}. Although we mainly discuss the mantle viscosity and GIA ice model for the melting rate of (0.69 ± 0.12) mm yr^{-1}, the results for the rate of (0.95 ± 0.17) mm yr^{-1} are essentially the same as those for the rate of (0.69 ± 0.12) mm yr^{-1}, particularly for the zonal rates of $n = 4$ and 6 (Figs 2 and 3).

We first discuss the GIA-induced secular rate of J_3 for the simple three-layer viscosity model (Figs 2 and 3). In Figs 2 and 3, the regions shown by orange and green colours indicate the permissible viscosity ranges inferred from the GIA-induced secular rates based on the geopotential zonal secular rates by Cheng *et al.* (1997) and Cox & Chao (2002), respectively. The GIA-induced $\dot{J}_3$ of –(2.8 ± 0.8) × 10^{-11} yr^{-1} based on the secular rate by Cheng *et al.* (1997) indicates the permissible viscosity solutions of η_{lm} ∼ (6–70) × 10^{21} Pa s, and η_{lm} ∼ (1–5) × 10^{22} and η_{um} ∼ (2–10) × 10^{20} Pa s for the IA10 and IR10 with an Antarctic ESL component (ESL_{SH}) of ∼10 m, respectively (Figs 2b and 3b). On the other hand, there is no permissible viscosity solution for GIA ice models with ESL_{SH} of ∼20 and ∼30 m.

We next examine the viscosity solution based on the estimate of –(0.6 ± 0.3) × 10^{-11} yr^{-1} derived from the $\dot{J}_3^{OBS}$ by Cox & Chao (2002). The permissible lower-mantle viscosities are smaller than 2 × 10^{21}, 4 × 10^{21} and 4 × 10^{21} Pa s for GIA ice models

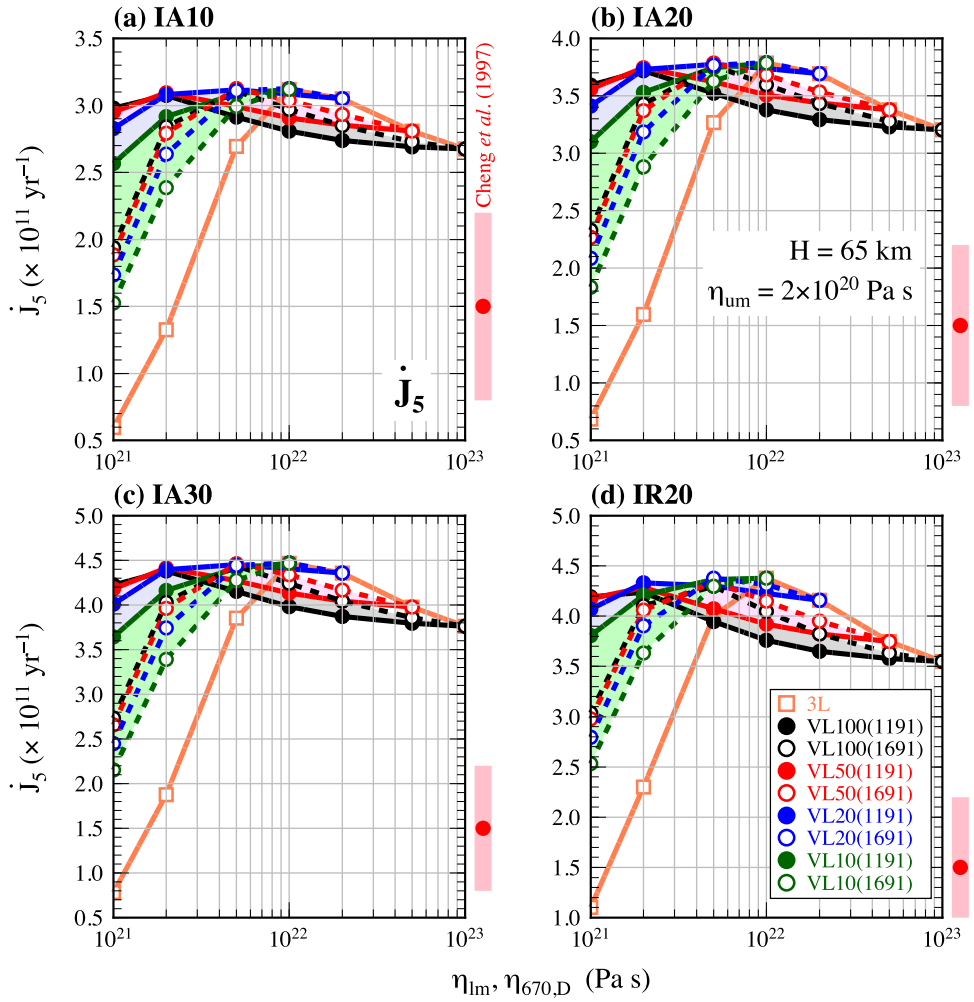

Figure 7. As in Fig. 5, except for the GIA-induced $\dot{J}_5$.

of IA10, IA20 and IR10, respectively (Figs 2b and h and 3b). On the other hand, the solutions for the IA30 and IR20 are $\eta_{lm} \sim$ (4–30) $\times 10^{21}$ and $\eta_{lm} > 10^{22}$ Pa s (Figs 2n and 3h), respectively, and there is no solution for the IR30 (Fig. 3n). The permissible lower-mantle viscosity generally increases with increasing ESL_{SH} value, and consequently, there is a trade-off between the viscosity solution and the melting history (period) and/or ESL component of the Antarctic ice sheet. This is related to the sensitivity of the $\dot{J}_3^{GIA}$ to the melting of the Antarctic ice sheet (Figs 4c and d). That is, change in $\dot{J}_3^{GIA}$ magnitude for the IA10 and IA30 (IR10 and IR30) is mainly attributed to the ESL component of the Antarctic ice model. On the other hand, the solutions for the IA30 and IR20 reflect the sensitivity of the $\dot{J}_3^{GIA}$ to the melting history of the Antarctic ice sheet that the rates for the IA30(S) ($ESL_{SH} \sim 30$ m) are nearly equal to those for the IR20(S) ($ESL_{SH} \sim 20$ m).

We consider the lumped-sum value for $\dot{J}_3$ and $\dot{J}_5$. The GIA-induced lumped-sum values by Cheng *et al.* (1997) shown in Table 2 provide the viscosity solutions similar to those for the geopotential zonal secular rate of J_3 by Cheng *et al.* (1997; Fig. 2b). For example, we consider the GIA-induced lumped-sum value based on the geodetic estimate by Starlette of $\dot{J}_3 + 1.04\ \dot{J}_5 \sim 2.1 \times 10^{-11}$ yr^{-1} (Table 2). For the IA10, the magnitude of GIA-induced zonal secular rate for $n = 3$ is nearly equal to that for $n = 5$, but the values are opposite each other (Figs 2b and d). That is, the GIA-induced lumped-sum value for these rates is consistent with the secular rate of $-(0.1 \pm 0.5) \times 10^{-11}$ yr^{-1} in Table 2. However, this is not true for the IR10 and the lumped-sum value is larger than 10^{-11} yr^{-1} (Figs 3b and d). Moreover, the lumped-sum values for other GIA ice models are larger than 2×10^{-11} yr^{-1} (Figs 2 and 3). On the other hand, the GIA-induced lumped-sum value of $-(1.6 \pm 0.6) \times 10^{-11}$ yr^{-1} based on the geodetic estimate by Devoti *et al.* (2001) may be inconsistent with the estimates in this study because the GIA-induced $\dot{J}_3 + 0.9\ \dot{J}_5$ value for all IA and IR ice models are positive (Figs 2 and 3).

Here, we shortly comment about the viscosity solutions for the two-layer lower-mantle viscosity model. Fig. 5 shows the GIA-induced $\dot{J}_3$ predicted for the two-layer lower-mantle viscosity model with $\eta_{um} = 2 \times 10^{20}$ Pa s and for IA10, IA20, IA30 and IR20 ice models. For the secular rate of $-(2.8 \pm 0.8) \times 10^{-11}$, we get the solutions for the IA10 as follows (Fig. 5a): $\eta_{670,D} < 10^{22}$ Pa s for $\eta_{D,2891} = 10^{23}$ Pa s (VL100), $\eta_{670,D} \leq 5 \times 10^{22}$ Pa s for $\eta_{D,2891} = 5 \times 10^{22}$ Pa s (VL50), $\eta_{670,D} \leq 2 \times 10^{22}$ Pa s for $\eta_{D,2891} = 2 \times 10^{22}$ Pa s (VL20) and $\eta_{670,D} \leq 10^{22}$ Pa s for $\eta_{D,2891} = 10^{22}$ Pa s (VL10). The viscosity solutions for the rate of $-(0.6 \pm 0.3) \times 10^{-11}$ yr^{-1} and the IR20 are as follows (Fig. 5d): $\eta_{670,D} > 10^{21}$ Pa s for $\eta_{D,2891} = 5 \times 10^{22}$ and 10^{23} Pa s and $\eta_{670,D} = (3–20) \times 10^{21}$ Pa s for $\eta_{D,2891} = 2 \times 10^{22}$ Pa s.

We discuss the permissible viscosity structure for the simple three-layer viscosity model based on the GIA-induced $\dot{J}_4$ of $-(2.4 \pm 1.2) \times 10^{-11}$ yr^{-1} derived from the geopotential zonal

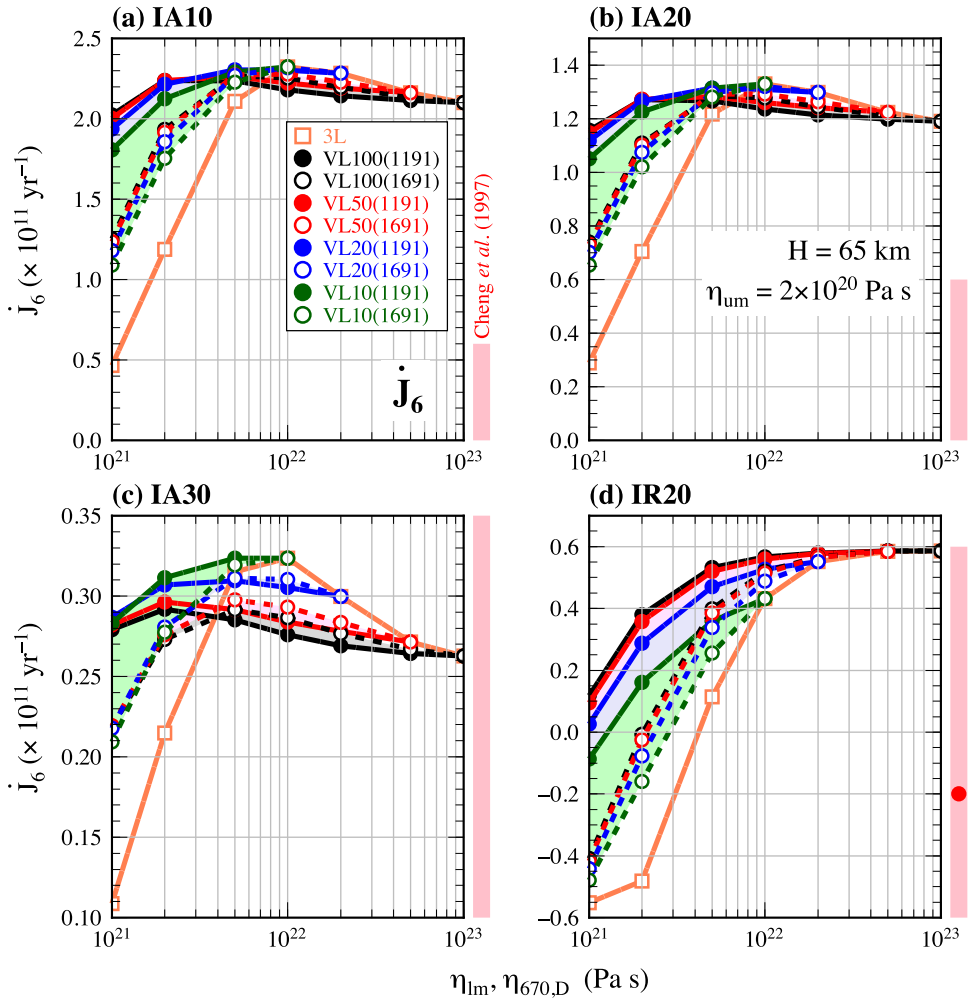

Figure 8. As in Fig. 5, except for the GIA-induced $\dot{J}_6$.

Table 2. Observationally derived, recent melting and GIA-induced values for the $\dot{J}_n$ ($n = 3$–6) and lumped-sum for $\dot{J}_3$ and $\dot{J}_5$ ($\times 10^{11}$ yr^{-1}). The contribution from recent melting of glaciers and Greenland and Antarctic ice sheets is based on the estimate for the period of 1900–1990 in Table 1. In the last column of this table, we also show the GIA-induced secular rates for the melting rate of (0.95 ± 0.17) mm yr^{-1} to discuss the effect of uncertainties of the melting rate for the period 1900–1990 on the inferred mantle viscosity (see the text).

Quantity	Observed rate	Rate for the recent melting	Rate for the GIA	Rate for the GIA by (0.95 ± 0.17) mm yr^{-1}
$\dot{J}_3$*	–1.3 ± 0.5	1.54 ± 0.31	–2.8 ± 0.8	–3.4 ± 0.9
$\dot{J}_3{}^a$	0.9	1.54 ± 0.31	–0.6 ± 0.3	–1.2 ± 0.4
$\dot{J}_3 - 0.27\dot{J}_5{}^b$	–2.1	1.38 ± 0.35	–3.5 ± 0.4	–4.0 ± 0.5
$\dot{J}_3 + 1.04\ \dot{J}_5{}^c$	2.1	2.15 ± 0.46	–0.1 ± 0.5	–0.9 ± 0.6
$\dot{J}_3 + 0.9\ \dot{J}_5{}^d$	0.5 ± 0.2	2.07 ± 0.44	–1.6 ± 0.6	–2.4 ± 0.8
$\dot{J}_4$*	–1.4 ± 1.0	1.02 ± 0.23	–2.4 ± 1.2	–2.8 ± 1.3
$\dot{J}_4{}^a$	–0.1	1.02 ± 0.23	–1.1 ± 0.2	–1.5 ± 0.3
$\dot{J}_5$*	2.1 ± 0.6	0.59 ± 0.14	1.5 ± 0.7	1.3 ± 0.8
$\dot{J}_6$*	0.3 ± 0.7	0.50 ± 0.11	–0.2 ± 0.8	–0.4 ± 0.9

*Cheng *et al.* (1997), [a]Cox & Chao (2002), [b]lumped-sum value by LAGEOS 1 (Cheng *et al.* 1997), [c]lumped-sum value by Starlette (Cheng *et al.* 1997) and [d]lumped-sum value by Starlette (Devoti *et al.* 2001).

secular rate of –(1.4 ± 1.0) × 10^{-11} yr^{-1} by Cheng *et al.* (1997). The contour maps for IA ice models indicate the permissible lower-mantle viscosities larger than 3×10^{21}, 2×10^{21} and 10^{21} Pa s for the IA10, IA20 and IA30, respectively (Figs 2c, i and o). Those for the IR10, IR20 and IR30 indicate the solutions of $\eta_{\rm lm} > 2 \times 10^{21}$, $\eta_{\rm lm} > 10^{21}$, and $\eta_{\rm lm} < 5 \times 10^{21}$ and $\eta_{\rm lm} > 4 \times 10^{22}$ Pa s, respectively (Figs 3c, i and o). That is, the GIA-induced secular rates predicted for most simple three-layer viscosity models are consistent with the $\dot{J}_4^{\rm GIA}$ value based on the geopotential zonal secular rate by Cheng *et al.* (1997). This is also true for the two-layer lower-mantle viscosity model, and the viscosity solutions for the IA10, IA20, IA30 and IR20 ice models are $\eta_{670,\rm D} \geq 10^{21}$ Pa s for $\eta_{\rm D,2891} = (1, 2, 5,$

10) $\times 10^{22}$ Pa s (Fig. 6). It should be important to note that the secular rates for these solutions, $-(2.4 \pm 1.2) \times 10^{-11}$ yr^{-1}, are largely attributed to the melting of the Antarctic ice sheet. That is, the NH contribution is significantly small compared with that for the SH one, and the sensitivity of the $\dot{J}_4^{\rm GIA}$ to GIA ice model is mainly determined by the viscous response to the melting of the Antarctic ice sheet (Figs 4e and f).

Here, we comment about the viscosity solution derived from the GIA-induced $\dot{J}_4$ of $-(1.1 \pm 0.2) \times 10^{-11}$ yr^{-1} based on the geopotential zonal secular rate by Cox & Chao (2002). For the simple three-layer viscosity model, the viscosity solution is $\eta_{\rm lm} < 3 \times 10^{21}$ Pa s regardless of adopted GIA ice models (Figs 2 and 3). However, the geodetically derived secular rate of J_4 for 1979–1992 by Cox & Chao (2002) is nearly the same as the estimate by Cheng *et al*. (1997). Then, the viscosity solution for the zonal secular rate by Cox & Chao (2002) would be similar to that for Cheng *et al*. (1997).

We discuss the viscosity solution for the GIA-induced $\dot{J}_5$ of $(1.5 \pm 0.7) \times 10^{-11}$ yr^{-1} derived from the geopotential zonal secular rate by Cheng *et al*. (1997). For the simple three-layer viscosity model, the permissible lower-mantle viscosity is (1–4) $\times 10^{21}$ Pa s for all GIA ice models (Figs 2 and 3). This solution is incompatible with the solution of $\eta_{\rm lm} > 6 \times 10^{21}$ Pa s for the IA10 and IR10 inferred from the GIA-induced $\dot{J}_3$ of $-(2.8 \pm 0.8) \times 10^{-11}$ yr^{-1} (Figs 2b and 3b). For the two-layer lower-mantle viscosity model, we get the solutions of $\eta_{670,1691} \sim 10^{21}$ Pa s and $\eta_{1691,2891} \geq 10^{22}$ Pa s for the IA10 and IA20 (Figs 7a and b).

We consider the $\dot{J}_6^{\rm GIA}$ for the simple three-layer viscosity model. The GIA-induced secular rate of $-(0.2 \pm 0.8) \times 10^{-11}$ yr^{-1} indicates the permissible viscosity solutions of $\eta_{\rm lm} < 2 \times 10^{21}$ Pa s for the IA10 and IA20, (1–100) $\times 10^{21}$ Pa s for the IA30, $\eta_{\rm lm} < 3 \times 10^{21}$ Pa s for the IR10, (1–100) $\times 10^{21}$ Pa s for the IR20, and $\eta_{\rm lm} < 2 \times 10^{21}$ and $\eta_{\rm lm} > 6 \times 10^{21}$ Pa s for the IR30. Generally, the permissible lower-mantle viscosity increases with increasing $\rm ESL_{SH}$ value, and there is a trade-off between the viscosity solution and the melting history and/or ESL component of the Antarctic ice sheet. This is related to the sensitivity of the $\dot{J}_6^{\rm GIA}$ to the melting of the Antarctic ice sheet (Figs 4i and j). For the two-layer lower-mantle viscosity model, the secular rates predicted for the IA30 and IR20 are consistent with the observationally derived rate (Figs 8c and d). The solutions for the IA30 and IR20 reflect the sensitivity of the $\dot{J}_6^{\rm GIA}$ to the melting history (period) of the Antarctic ice sheet that the rates for the IA30(S) are nearly equal to those for the IR20(S).

Before making comprehensive arguments for the inferred mantle viscosity from each $\dot{J}_n^{\rm GIA}$, we point out the differences between the inferred viscosity solutions for this study and Tosi *et al*. (2005) because the approach by Tosi *et al*. (2005) is essentially the same as that adopted here. Tosi *et al*. (2005) inferred the mantle viscosity based on the analyses using the observationally derived zonal secular rates mainly up to degree 6 (Cheng *et al*. 1997), the ICE3G with the Antarctic ESL component of ∼25 m during 10–5 kyr BP and recent melting of the Antarctic and Greenland ice sheets before 1995. The recent melting areas differ from those for this study (see recent melting model for the period of 1900–1990 in Table 1). They adopted the forward method for each even and odd zonal secular rate as adopted in this study, and also inverse method using a classical χ^2 analysis to infer the mantle viscosity and recent melting by minimizing the misfit between the observed and predicted $\dot{J}_n$ ($n = 2$–6). Although an average lower-mantle viscosity of $\sim 10^{22}$ Pa s for the inverse analysis is quite consistent with that based on the $\dot{J}_2^{\rm GIA}$ by Nakada *et al*. (2015), it is difficult to compare their viscosity solution with that for the forward analysis in this study. It is also noted that the optimal melting rates for the Antarctic and Greenland ice sheets before 1995 are 0.8 and 0.2 mm yr^{-1}, respectively (Tosi *et al*. 2005).

The forward analysis by Tosi *et al*. (2005) indicates that the main difference between the inferred viscosity solutions for both studies is attributed to the recent melting model as described below. It would be acceptable to discuss the difference by assuming the melting model before 1990. This study assumes recent melting from glaciers and peripheral glaciers for the Greenland ice sheet (Table 1), but Tosi *et al*. (2005) assume the melting for the Antarctic and Greenland ice sheets. The recent melting components of the zonal secular rates for $n = 3$ and 5 based on the melting rate of 0.7 mm yr^{-1} from the Antarctic ice sheet are negative and -2.8×10^{-11} and -2.3×10^{-11} yr^{-1}, respectively (see table 4 in Tosi *et al*. 2005 and also their table 5 for the melting model with melting rates of 0.8 and 0.2 mm yr^{-1} for the Antarctic and Greenland ice sheets, respectively), which are also consistent with the estimates based on the Antarctic melting for the period of 2002–2011 (Table 2). However, the zonal secular rates for this study are positive and ∼1.5 and ∼0.6 $\times 10^{-11}$ yr^{-1} because of the melting from glaciers and peripheral glaciers for the Greenland ice sheet (Table 1), and the magnitude is significantly smaller than that for Tosi *et al*. (2005). On the other hand, the recent melting components of the zonal secular rates for $n = 2$, 4 and 6 are positive in both studies regardless of the melting areas, and both studies suggest similar viscosity solutions for the simple three-layer viscosity model (Figs 2 and 3). For example, the analyses for $n = 2$ and 4 based on the ICE3G and Antarctic melting rate of 0.7 mm yr^{-1} by Tosi *et al*. (2005) indicate two permissible lower-mantle viscosities; $\eta_{\rm lm} \leq 10^{22}$ and $\eta_{\rm lm} > 10^{22}$ Pa s (fig. 3 in Tosi *et al*. 2005), which are not inconsistent with our viscosity solutions for GIA ice models of IR20 ($\rm ESL_{SH} \sim 20$ m) and IR30 ($\rm ESL_{SH} \sim 30$ m) (Figs 2 and 3). That is, the difference between the inferred viscosity solutions for this study and Tosi *et al*. (2005), particularly for the odd zonal secular rates of $n = 3$ and 5, is mainly attributed to the recent melting models adopted in both studies.

We come back to the discussion for the results obtained in this study. The GIA-induced zonal secular rates, $\dot{J}_n^{\rm GIA}$ ($n = 3$–6), derived from the available geopotential zonal secular rates, $\dot{J}_n^{\rm OBS}$ (e.g. Cheng *et al*. 1997; Cox & Chao 2002) and the recent melting contribution, $\dot{J}_n^{\rm RM}$, based on the melting of glaciers and the Greenland and Antarctic ice sheets (Vaughan *et al*. 2013) cannot put tight constraints on the $\eta_{670,\rm D}$ and $\eta_{\rm D,2891}$ values as noted earlier in this section. It is true even if we adopt the $\dot{J}_n^{\rm GIA}$ for the recent melting rate (ESLR) of (0.95 ± 0.17) mm yr^{-1} considering uncertainties of the melting rate for the period of 1900–1990 on the inferred mantle viscosity (Figs 2 and 3). However, it is possible to point out the importance of the $\dot{J}_n^{\rm OBS}$ ($n > 2$) on inference of mantle viscosity and GIA ice model, particularly for Antarctic melting history due to the last deglaciation. We discuss this point by taking into account the results based on the two-layer lower-mantle viscosity by Nakada & Okuno (2016). The GIA-induced $\dot{J}_2$ provides two permissible lower-mantle viscosities for the simple three-layer viscosity model, $\sim 10^{22}$ and (5–10) $\times 10^{22}$ Pa s, regardless of adopted GIA ice models (Figs 2 and 3 and also Nakada *et al*. 2016). Here, we assume that the lower-mantle viscosity for the simple three-layer viscosity model is given by either of the lower-mantle viscosities inferred from the $\dot{J}_2^{\rm GIA}$. For the two-layer lower-mantle viscosity model, we adopt two viscosity solutions inferred from the GIA-induced $\dot{J}_2$, LGM sea level constraints and postglacial differential RSL change (Nakada

& Okuno 2016); namely, $\eta_{670,1191} > 3 \times 10^{21}$ Pa s for $\eta_{1191,2891} = (5–10) \times 10^{22}$ Pa s and $\eta_{670,1691} > 10^{22}$ Pa s for $\eta_{1691,2891} = (5–10) \times 10^{22}$ Pa s, in which the upper-mantle viscosity is $(1–4) \times 10^{20}$ Pa s for both viscosity models. These viscosity models are referred to as VS1191 and VS1691, respectively.

We first discuss the mantle viscosity and GIA ice model inferred from the GIA-induced even zonal secular rates of $n = 4$ and 6. The solutions for the recent melting rate of (0.95 ± 0.17) mm yr^{-1} are nearly the same as those for the rate of (0.69 ± 0.12) mm yr^{-1} (Figs 2 and 3). For the simple three-layer viscosity model, the viscosity solutions for the $\dot{J}_2^{\rm GIA}$ are comprised in the viscosity solutions for the IR20 and IA30 based on the GIA-induced even zonal secular rates ($n = 4$ and 6) using the geopotential zonal secular rates by Cheng *et al*. (1997), and the solution of $(5–10) \times 10^{22}$ Pa s is obtained for the IR30 (Figs 2 and 3). This may be true for the $\dot{J}_4^{\rm GIA}$ value from the geopotential zonal secular rate for the period of 1979–1992 by Cox & Chao (2002). For the two-layer lower-mantle viscosity model, the zonal secular rates predicted for the IR20 and IA30 satisfy the observationally derived $\dot{J}_4^{\rm GIA}$ and $\dot{J}_6^{\rm GIA}$ regardless of $\eta_{670,\rm D}$ and $\eta_{\rm D,2891}$ values adopted here (Figs 6c and d, and 8c and d). This is true for the IR30 although we do not show the results here. For example, the permissible viscosity solutions for the IR20 are $\eta_{670,\rm D} = (1–100) \times 10^{21}$ Pa s for $\eta_{\rm D,2891} = (5–10) \times 10^{22}$ Pa s, which comprise the permissible viscosity ranges for VS1191 and VS1691. The solutions for the IA30 and IR20 reflect the sensitivity of GIA-induced zonal secular rates to the melting history of the Antarctic ice sheet as previously stated. That is, if the melting history due to the last deglaciation is wholly represented by GIA ice model such as the IR20 with $\rm ESL_{SH} \sim 20$ m or IA30 with $\rm ESL_{SH} \sim 30$ m, then the observationally derived GIA-induced even zonal secular rates ($n = 2$, 4 and 6) provide consistent viscosity solutions for the two-layer lower-mantle viscosity model. Such GIA ice models may also be supported from the postglacial RSL changes at Southport and Bermuda located on the intermediate region of North American ice sheets (Nakada & Okuno 2016).

We consider GIA-induced odd zonal secular rates of $n = 3$ and 5. The simple three-layer viscosity models satisfying the observationally derived $\dot{J}_5^{\rm GIA}$ are inconsistent with the solutions inferred from the $\dot{J}_2^{\rm GIA}$ (Figs 2 and 3). This is also true for the two-layer lower-mantle viscosity model (Fig. 7). On the other hand, the viscosity solutions for the IA10 and IR10 ($\rm ESL_{SH} \sim 10$ m) based on the $\dot{J}_3^{\rm GIA}$ using the geopotential zonal secular rate by Cheng *et al*. (1997) satisfy the viscosity solutions inferred from the $\dot{J}_2^{\rm GIA}$ in both the simple three-layer and two-layer lower-mantle viscosity models (Figs 2, 3 and 5a). The viscosity solutions for the two-layer lower-mantle viscosity model are, for example, $\eta_{670,\rm D} > 10^{21}$ Pa s for $\eta_{\rm D,2891} = 5 \times 10^{22}$ Pa s and $\eta_{670,1691} < 2 \times 10^{22}$ Pa s for $\eta_{1691,2891} = 10^{23}$ Pa s (Fig. 5a). For the $\dot{J}_3^{\rm OBS}$ by Cox & Chao (2002), the viscosity solutions for the IA30 and IR20 satisfy the solutions for the $\dot{J}_2^{\rm GIA}$ (Figs 2n, 3h and 5c and d). For example, the solutions for the IR20 in the two-layer lower-mantle viscosity model are $\eta_{670,\rm D} > 2 \times 10^{21}$ Pa s for $\eta_{\rm D,2891} = (5–10) \times 10^{22}$ Pa s (Fig. 5d). However, it would be safe to say that the viscosity solutions derived from the odd zonal secular rates are left open if we consider uncertainties of the geopotential odd zonal secular rates based on the SLR observations (Cheng *et al*. 1997).

5 CONCLUDING REMARKS

We examined the GIA-induced $\dot{J}_n$ ($n \geq 2$) derived from the geopotential zonal secular rates (Cheng *et al*. 1997; Devoti *et al*. 2001; Cox & Chao 2002) and recent melting by Vaughan *et al*. (2013) to explore the possibility of additional information on the lower-mantle viscosity solutions, VS1191 and VS1691, and GIA ice model inferred from the analyses of the $\dot{J}_2^{\rm GIA}$ and RSL changes by Nakada & Okuno (2016) (see also Lau *et al*. 2016). The GIA-induced zonal secular rates for $n \geq 2$ provide important constraints on the lower-mantle viscosity and the Antarctic melting history (Ivins *et al*. 1993; Mitrovica & Peltier 1993; Devoti *et al*. 2001; Tosi *et al*. 2005), and particularly, the rates for $n = 3$ and 4 are mainly attributed to the viscous response of the lower mantle to the melting of the Antarctic ice sheet largely characterized by the ESL component ($\rm ESL_{SH}$) and the melting period of the Antarctic ice sheet (Fig. 4).

The analyses of the $\dot{J}_n^{\rm GIA}$ ($n > 2$) based on the geopotential zonal secular rates by Cheng *et al*. (1997) suggest different lower-mantle viscosity solutions for the even and odd zonal secular rates (Figs 2, 3 and 5–8). For the Antarctic ice model with $\rm ESL_{SH}$ of ∼20 or ∼ 30 m (IR20 or IA30), the viscosity solutions satisfying both $\dot{J}_4^{\rm GIA}$ and $\dot{J}_6^{\rm GIA}$ values comprise the permissible viscosity ranges for VS1191 and VS1691 (Figs 6 and 8). On the other hand, there is no viscosity solution satisfying $\dot{J}_3^{\rm GIA}$ and $\dot{J}_5^{\rm GIA}$ values (Figs 5 and 7). For the GIA-induced secular rate of $n = 3$, however, it may be noted that the permissible viscosity ranges for the VS1191 and VS1691 are obtained for the IA10 ($\rm ESL_{SH} \sim 10$ m) in the case of the $\dot{J}_3^{\rm GIA}$ based on the negative geopotential zonal secular rate by Cheng *et al*. (1997) (Fig. 5a), while such permissible viscosity solutions are obtained for the IR20 ($\rm ESL_{SH} \sim 20$ m) if we adopt the $\dot{J}_3^{\rm GIA}$ based on the positive secular rate by Cox & Chao (2002; Fig. 5d). These results are true for the GIA-induced $\dot{J}_n^{\rm GIA}$ ($n > 2$) for the melting rates of (0.69 ± 0.12) and (0.95 ± 0.17) mm yr^{-1} considering uncertainties of the melting rate for the period of 1900–1990. Although we cannot give a persuasive evaluation on the discrepancy between the solutions for the even and odd zonal secular rates, the discrepancy may probably arise from the incomplete modeling of GIA ice model, uncertainties of the geopotential zonal secular rates based on the SLR data and particularly those for odd zonal secular rates due to weakness in the orbital geometry (Cheng *et al*. 1997) and also uncertainties in the assumed recent melting rates.

In this study, we mainly discussed the mantle viscosity and GIA ice model based on the GIA-induced $\dot{J}_n$ ($n > 2$) inferred from the assumed recent melting rates and geopotential zonal secular rates before 1990 because the zonal secular rates for $n > 2$ may be available only for the period of 1976–2002 as far as we know. However, there is no doubt that the analyses using temporal variations in zonal secular rates for the period of 1976–2011 [see variations in secular rates for $n = 2$ by Roy & Peltier (2011) and Cheng *et al*. (2013)] would provide more tight constraints on mantle viscosity as was indicated for the $\dot{J}_2$ by Nakada *et al*. (2015) (see also Mitrovica *et al*. 2015). If the secular rates for $n > 2$ are available for such a period, then we would really like to analyse the $\dot{J}_n^{\rm GIA}$ ($n > 2$) based on the geopotential zonal secular rates for separate periods such as 2002–2011 and before 1990. That is, the even zonal secular rates for the period of 2002–2011 are about three times as large as than those before 1990, while such a significant change is not expected for the secular rates of $n = 3$ and 5 (Table 1) in the assumed recent melting rates. Such analyses would help to evaluate uncertainties of the recent melting rate as well as those for the geopotential zonal secular rates more persuasively, and consequently it may be possible to put additional constraints on the lower-mantle viscosity structure inferred from the analyses of the $\dot{J}_2^{\rm GIA}$ and RSL changes and also GIA ice model, particularly for the Antarctic melting history due to the last deglaciation.

ACKNOWLEDGEMENTS

We thank two anonymous reviewers and the editor (L.L.A. Vermeersen) for their constructive comments. This work was partly supported by the Japanese Ministry of Education, Science and Culture (grand-in-aid for scientific research no. 16K05543).

REFERENCES

Bard, E., Hamelin, B., Arnold, M., Montaggioni, L., Cabioch, G., Faure, G. & Rougerie, F., 1996. Deglacial sea-level record from Tahiti corals and timing of global meltwater discharge, *Nature,* **382,** 241–244.

Cambiotti, G., Ricard, Y. & Sabadini, R., 2011. New insights into mantle convection true polar wander and rotational bulge readjustment, *Earth planet. Sci. Lett.,* **310,** 538–543.

Cambiotti, G., Wang, X., Sabadini, R. & Yuen, D.A., 2016. Residual polar motion caused by coseismic and interseismic deformations from 1900 to present, *Geophys. J. Int.,* **205,** 1165–1179.

Cazenave, A., Gegout, P. & Ferhat, G., 1996. Secular variations of the gravity field from Lageos 1, Lageos 2 and Ajisai, in *Global Gravity Field and its Temporal Variations, Int. Assoc. Geod. Symp*., Vol. 116, pp. 141–151, Springer-Verlag, New York.

Chappell, J., Chivas, A., Wallensky, E., Polach, H.A. & Aharon, P., 1983. Holocene paleo-environmental changes, central to north Great Barrier Reef inner zone, *Bur. Min. Res. J. Aust. Geol. Geophys.,* **8,** 223–235.

Cheng, M.K, Tapley, B.D. & Ries, J.C., 2013. Deceleration in the Earth's oblateness, *J. geophys. Res.,* **118,** 740–747.

Cheng, M.K., Shum, C.K. & Tapley, B.D., 1997. Determination of long-term changes in the Earth's gravity field from satellite laser ranging observations, *J. geophys. Res.,* **102,** 22 377–22 390.

Cheng, M.K., Tapley, B.D., Eanes, R.J. & Shum, C.K., 1993. Time-varying gravitational effects from analysis of measurements from geodetic satellite (abstract), *EOS, Trans. Am. geophys. Un.,* **74,** 196.

Cheng, M.K., Eanes, R.J., Shum, C.K., Schutz, B.E. & Tapley, B.D., 1989. Temporal variations in low degree zonal harmonics from Starlette orbital analysis, *Geophys. Res. Lett.,* **16,** 393–396.

Cox, C.M. & Chao, B.F., 2002. Detection of a large-scale mass redistribution in the terrestrial system since 1998, *Science,* **297,** 831–833.

Deschamps, P. *et al.*, 2012. Ice-sheet collapse and sea-level rise at the Bolling warming 14,600 years ago, *Nature,* **483,** 559–564.

Devoti, R., Luceri, V., Sciarretta, C., Bianco, G., Di Donato, G., Vermeersen, L.L.A. & Sabadini, R., 2001. The SLR secular gravity variations and their impact on the inference of mantle rheology and lithospheric thickness, *Geophys. Res. Lett.,* **28,** 855–858.

Dziewonski, A.M. & Anderson, D.L., 1981. Preliminary reference Earth model (PREM), *Phys. Earth planet. Inter.,* **25,** 297–356.

Fairbanks, R.G., 1989. A 17,000 year glacio-eustatic sea level record: influence of glacial melting rates on the Younger Dryas event and deep ocean circulation, *Nature,* **342,** 637–641.

Ivins, E.R., Sammis, C.G. & Yoder, C.F., 1993. Deep mantle viscous structure with prior estimate and satellite constraint, *J. geophys. Res.,* **98,** 4579–4609.

Ivins, E.R., James, T.S., Wahr, J., Schrama, E.J.O., Landerer, F.W. & Simon, K.M., 2013. Antarctic contribution to sea level rise observed by GRACE with improved GIA correction, *J. geophys. Res.,* **118,** 1–16.

Lambeck, K., 1993. Glacial rebound of the British Isles – I. Preliminary model results, *Geophys. J. Int.,* **115,** 941–959.

Lambeck, K., Rouby, H., Purcell, A., Sun, Y. & Sambridge, M., 2014. Sea level and global ice volumes from the last glacial maximum to the Holocene, *Proc. Natl. Acad. Sci.,* **111,** 15 296–15 303.

Lau, H.C.P., Mitrovica, J.X., Austermann, J., Crawford, O., Al-Attar, D. & Latychev, K., 2016. Inference of mantle viscosity based on ice age data sets: radial structure, *J. geophys. Res.,* **121,** doi:10.1002/2016JB013043.

Mitrovica, J.X., 1996. Haskell [1935] revisited, *J. geophys. Res.,* **101,** 555–569.

Mitrovica, J.X. & Forte, A.M., 2004. A new inference of mantle viscosity based upon joint inversion of convection and glacial isostatic adjustment data, *Earth planet. Sci. Lett.,* **225,** 177–189.

Mitrovica, J.X. & Peltier, W.R., 1993. Present-day secular variations in the zonal harmonics of the Earth's geopotential, *J. geophys. Res.,* **98,** 4509–4526.

Mitrovica, J.X., Hay, C.C., Morrow, E., Kopp, R.E., Dumberry, M. & Stanley, S., 2015. Reconciling past changes in Earth's rotation with 20th century global sea-level rise: resolving Munk's enigma, *Sci. Adv,* **1,** doi:10.1126/sciadv. 1500679.

Nakada, M. & Lambeck, K., 1988. The melting history of the Late Pleistocene Antarctic ice sheet, *Nature,* **333,** 36–40.

Nakada, M. & Lambeck, K., 1989. Late Pleistocene and Holocene sea-level change in the Australian region and mantle viscosity, *Geophys. J. Int.,* **96,** 497–517.

Nakada, M. & Okuno, J., 2003. Perturbations of the Earth's rotation and their implications for the present-day mass balance of both polar ice caps, *Geophys. J. Int.,* **152,** 124–138.

Nakada, M. & Okuno, J., 2016. Inference of mantle viscosity for depth resolutions of GIA observations, *Geophys. J. Int.,* **207,** 719–740.

Nakada, M., Okuno, J. & Yokoyama, Y., 2016. Total meltwater volume since the Last Glacial Maximum and viscosity structure of Earth's mantle inferred from relative sea level changes at Barbados and Bonaparte Gulf and GIA-induced $\dot{J}_2$, *Geophys. J. Int.,* **204,** 1237–1253.

Nakada, M., Okuno, J., Lambeck, K. & Purcell, A., 2015. Viscosity structure of Earth's mantle inferred from rotational variations due to GIA process and recent melting events, *Geophys. J. Int.,* **202,** 976–992.

Nakada, M., Kimura, R., Okuno, J., Moriwaki, K., Miura, H. & Maemoku, K., 2000. Late Pleistocene and Holocene melting history of the Antarctic ice sheet derived from sea-level variations, *Mar. Geol.,* **267,** 85–103.

Nakiboglu, S.M. & Lambeck, K., 1980. Deglaciation effects upon the rotation of the Earth, *Geophys. J. R. astr. Soc.,* **622,** 49–58.

Nerem, R.S. & Klosko, S.M., 1996. Secular variations of the zonal harmonics and polar motions as geophysical constraints, in *Global Gravity Field and its Temporal Variations, Int. Assoc. Geod. Symp.*, Vol. 116, pp. 152–163, Springer-Verlag, New York.

Paterson, W.S.B., 1971. *The Physics of Glaciers,* Pergamon.

Peltier, W.R., 1988. Global sea level rise and Earth rotation, *Science,* **240,** 895–901.

Peltier, W.R., 2004. Global glacial isostasy and the surface of the ice-age earth: the ICE-5G(VM2) model and GRACE, *Annu. Rev. Earth planet. Sci.,* **32,** 111–149.

Peltier, W.R., 2007. History of Earth rotation, in *Evolution of the Earth, Treatise on Geophysics*, Vol. 9, pp. 243–293, ed. Stevenson, D., Elsevier, Amsterdam.

Peltier, W.R. & Fairbanks, R.G., 2006. Global glacial ice volume and Last Glacial Maximum duration from an extended Barbados sea level record, *Quat. Sci. Rev.,* **25,** 3322–3337.

Roy, K. & Peltier, W.R., 2011. GRACE era secular trends in Earth rotation parameters: a global scale impact of the global warming process?, *Geophys. Res. Lett.,* **38,** doi:10.1029/2011GL047282.

Rubincam, D.P., 1984. Postglacial rebound observed by LAGEOS and the effective viscosity of the lower mantle, *J. geophys. Res.,* **89,** 1977–1987.

Sabadini, R., Yuen, D.A. & Boschi, E., 1982. Polar wandering and forced responses of a rotating, multilayered, viscoelastic planet, *J. geophys. Res.,* **87,** 2885–2903.

Sabadini, R., Yuen, D.A. & Gasperini, D.A., 1988. Mantle rheology and satellite signatures from present-day glacial forcings, *J. geophys. Res.,* **93,** 437–447.

Tosi, N., Sabadini, R., Marotta, A.M. & Vermeersen, L.L.A., 2005. Simultaneous inversion for the Earth's viscosity and ice mass imbalance in Antarctica and Greenland, *J. geophys. Res.,* **110,** doi:10.1029/2004JB003236.

Tushingham, A.E. & Peltier, W.R., 1991. ICE-3G: a new global model of late Pleistocene deglaciation based on geophysical predictions of post-glacial relative sea level change, *J. geophys. Res.,* **96,** 4497–4523.

Vaughan, D.G. *et al.*, 2013. Observations: Cryosphere, in Climate Change 2013: *The Physical Science Basis, Contribution of Working Group I to the Fifth Assessment Report of the Intergovernmental Panel on Climate*

Change, pp. 317–382, eds Stocker, T.F. *et al.*, Cambridge Univ. Press, Cambridge, UK/New York, NY, USA.

Vermeersen, L.L.A., Fournier, A. & Sabadini, R., 1997. Changes in rotation induced by Pleistocene ice masses with stratified analytical Earth models, *J. geophys. Res.,* **102,** 27 689–27 702.

Whitehouse, P.L., Bentley, M.J. & Le Brocq, A.M., 2012. A deglacial model for Antarctica: geological constraints and glaciological modelling as a basis for a new model of Antarctic glacial isostatic adjustment, *Quat. Sci. Rev.,* **32,** 1–24.

Wu, P. & Peltier, W.R., 1983. Glacial isostatic adjustment and the free air gravity anomaly as a constraint on deep mantle viscosity, *Geophys. J. R. astr. Soc.,* **74,** 377–450.

Wu, P. & Peltier, W.R., 1984. Pleistocene deglaciation and the Earth's rotation: a new analysis, *Geophys. J. R. astr. Soc.,* **76,** 753–791.

Yoder, C.F., Williams, J.G., Dickey, J.O., Schutz, B.E., Eanes, R.J. & Tapley, B.D., 1983. $\dot{J}_2$ from LAGEOS and nontidal acceleration of Earth rotation, *Nature,* **303,** 757–762.

Yokoyama, Y., Lambeck, K., De Deckker, P., Johnston, P. & Fifield, L.K., 2000. Timing of the Last Glacial Maximum from observed sea-level minima, *Nature,* **406,** 713–716.

Yuen, D.A., Sabadini, R. & Boschi, V., 1982. Viscosity of the lower mantle as inferred from rotational data, *J. geophys. Res.,* **87,** 10 745–10 762.